

PHYSIO-CHEMICAL DEGRADATION OF CONCRETE:
A RAMIFICATION OF COUPLED FREEZE-THAW AND SULFATE ATTACK

by
MD Aminul Islam

A thesis
submitted in partial fulfillment
of the requirements for the degree of
Master of Science in Civil Engineering
Boise State University

December 2018

© 2018

MD Aminul Islam

ALL RIGHTS RESERVED

BOISE STATE UNIVERSITY GRADUATE COLLEGE

DEFENSE COMMITTEE AND FINAL READING APPROVALS

of the thesis submitted by

MD Aminul Islam

Thesis Title: Physio-Chemical Degradation of Concrete: A Ramification of Coupled Freeze-Thaw and Sulfate Attack

Date of Final Oral Examination: 12 November 2018

The following individuals read and discussed the thesis submitted by student Md Aminul Islam, and they evaluated his presentation and response to questions during the final oral examination. They found that the student passed the final oral examination.

Yang Lu, Ph.D. Chair, Supervisory Committee

Debakanta Mishra, Ph.D. Member, Supervisory Committee

Lan Li, Ph.D. Member, Supervisory Committee

The final reading approval of the thesis was granted by Yang Lu, Ph.D., Chair of the Supervisory Committee. The thesis was approved by the Graduate College.

DEDICATION

To my real friends, my parents.

ACKNOWLEDGEMENTS

First and foremost, I would like to express my sincere gratitude to my advisor, Dr. Yang Lu, who always encourages me to do innovative research. His welcoming nature, kind appreciation, timely feedback and unparalleled guidance motivate me to reach my extreme ability for achieving the required goal. It is him who helped me to stay on course by shedding light when I was lost during my research studies. I am also grateful to Dr. Mishra, and Dr. Lan Li for their immense support during my thesis work.

My appreciation is due to Saif Al Mahmud for being an awesome little brother and a roommate. I cannot repay the invaluable mental support I got from him during last six months. I am also thankful to other NBGS members Al Amin Ahmed Simon, Nabil Rahman, Maruf Ahmed, Touhidul Islam and the one and only A-Beer Ashfaque Rahman. Life would be a nightmare if you guys were not around. Last but not least, I am indebted for the help I received from Aidin Jafary Golrokh, my long term researchmate in MMSIG research group in Boise State CE department.

Finally, I am highly thankful to the Civil Engineering department of Boise State University for accepting my application in the first place. I am also thankful to the administrative assistant Rhonda Magill for always being there to help all the graduate students from the beginning.

ABSTRACT

Concrete structures experience damage due to Sulfate Attack (SA) and Freeze-Thaw (F-T) in cold regions containing ample amount of sulfate species. The combined effect of SA and F-T is a multiscale multiphysics damaging process for cementitious materials involving complicated chemical reactions and phase transition inside concrete pores. This thesis is a compilation of two theoretical models describing the SA induced damage in an unsaturated cementitious medium and damage due to the combined effect of SA and F-T. The classical theory of phase change and a diffusion-reaction process is utilized in the development of the models. The validity of the proposed models is tested by comparing the numerical results against existing experimental data for concrete mortars. It is found that the numerical results agree very well with the experimental results. These coupled mathematical models can be applied to assess the effect of ambient sulfate concentration on the degradation of concrete, the pore-size distribution (PSD), hysteresis of solidification and melting of water in concrete pores and change of porosity due to SA and F-T. Most importantly the proposed mathematical model is capable of explaining the damage extent of concrete under coupled conditions that are somewhat difficult and time consuming to be evaluated by contemporary experimental methods.

TABLE OF CONTENTS

DEDICATION	iv
ACKNOWLEDGEMENTS	v
ABSTRACT	vi
TABLE OF CONTENTS.....	vii
LIST OF TABLES	x
LIST OF FIGURES	xi
CHAPTER ONE: INTRODUCTION	1
Research objective	2
Outline of this thesis	3
REFERENCES.....	5
CHAPTER TWO: CHEMO-MECHANICAL MODELING OF SULFATE ATTACK- INDUCED DAMAGE PROCESS IN CEMENT STABILIZED PAVEMENTS	6
Abstract	6
Introduction	7
Research Objective	10
Chemo-mechanical Mechanisms of Sulfate Attack	11
Mass Balance	12
Sulfate Attack in Unsaturated Sample	14
Effect of Heat on Sulfate Attack.....	16
Heat Transport in Cement Stabilized Subgrade.....	19
Governing Equations for Coupled CM Behavior Under SA.....	22

Mechanical Damage due to Sulfate Attack	23
Results and Discussion.....	27
Validation of the Proposed Model	27
Sulfate, Moisture and Heat Migration.....	33
Case Study	37
Conclusion.....	42
REFERENCES.....	44
CHAPTER THREE: COUPLED THERMO-CHEMO-MECHANICAL MODELLING OF CONCRETE DURABILITY SUBJECTED TO COMBINED SULFATE ATTACK AND FREEZE-THAW CONDITIONS	47
Abstract	47
Introduction	48
Coupled F-T and SA Equation Set Derivation	56
Freezing Theory of Porous Structures	56
Phase Transition in Pores.....	61
Mass Transport.....	64
Modeling Stress and Strain	66
Governing Equations for Coupled TCM Behavior Under SA and FT	68
Model Validation	69
Results and Discussion.....	76
Variation in Temperature at The Center of the Specimen	76
Hysteresis of Solidification and Melting Due to Freeze-Thaw.....	78
Variation of Sulfate Concentration Due to F-T Damage.....	80
Conclusion.....	81

REFERENCES.....	83
CHAPTER FOUR: CONCLUSION	87

LIST OF TABLES

Table 2-1.	Initial and boundary condition for the simulation.....	28
Table 2-2.	Parameters used for the simulation	29
Table 3-1.	Initial and boundary conditions.....	72
Table 3-2.	Material properties	73
Table 3-3.	Final porous ice content.....	76

LIST OF FIGURES

Figure 2-1.	Flow diagram of the solution procedure of the proposed model...	11
Figure 2-2.	Variation of sulfate diffusion coefficient with temperature.....	17
Figure 2-3.	Variation of sulfate diffusion coefficient	18
Figure 2-4.	Qualitative diagram of variation of expansion strain with time	24
Figure 2-5.	Simulation domain showing dimension and boundary numbers...	27
Figure 2-6.	Validation of the proposed model	30
Figure 2-7.	Changes in concentration of sulfate and aluminate inside cementitious materials	32
Figure 2-8.	(A) Propagation of Sulfate inside cement stabilized subgrade at 0, 30, 60 and 90 days. (B) Distribution of sulfate concentration (<i>mol/m³</i>) at 90 days.	34
Figure 2-9.	(A) Variation of the degree of saturation with time, (B) Variation of temperature with time	36
Figure 2-10.	Schematic diagram of the model adopted for a case study	38
Figure 2-11.	Simulation results at one month: (A) Variation of Degree of saturation, (B) Variation of Temperature (K)	39
Figure 2-12.	Simulation results at four months: (A) Sulfate migration inside concrete, (B) Stress induced by diffused sulfate (psi) (C) Stress induced by diffused sulfate (mm/mm)	40
Figure 2-13.	Failure indicated by DP yield criterion	41
Figure 3-1:	Concept map of interaction between SA and F-T	49
Figure 3-2.	Pore size distribution of concrete with w/c ratios of 0.3 and 0.5 (This plot was drawn by extracting PSD data from Gong et al.(Gong et al., 2014))	70

Figure 3-3.	a) Full-size mortar sample, b) Simulation domain for validating the proposed model	71
Figure 3-4.	Ice fraction in mortar sample with, a) Sample1 and b) Sample2 ..	74
Figure 3-5.	Freezing with and without sulfate attack.	77
Figure 3-6.	Hysteresis of solidification and melting due to fluctuation in temperature in pores.....	79
Figure 3-7.	Effect of F-T damage on sulfate concentration inside concrete	80

CHAPTER ONE: INTRODUCTION

Concrete is a highly heterogeneous material consisting of aggregates, cement-based binder and water. Usage of cement concrete began in ancient Rome. After the introduction of metal reinforcements in concrete and due to being economical, this material has become one of the most consumed materials in building constructions around the world. Concrete structures have been constructed in diverse environmental conditions. The durability of concrete becomes a concern while placing it in predominantly harsh external conditions due to several deleterious chemical and physical processes. These environmental degradation phenomena (chemical and physical) can substantially reduce the load-bearing capacity and functionality (loss of stiffness, cracking, spalling) of concrete structures. Chemical degradation process can result from chemical reactions triggered by external ions after being penetrated into concrete pores. Such chemical reactions can result from chloride or sulfate ions or from slow expansive reactions among the components of the concrete as in the case of an alkali-silica reaction. In contrast, physical damage may occur from thermal fatigue, high temperature in case of fire damage, and damage due to Freeze-Thaw. All these deterioration types are also highly reliant on the porous structure of concrete as well as on the extent of chemical reactions. While new structures may be designed for aggressive environments to keep the structure from physio-chemical degradation that can be mitigated by the use of special cement or additives, the inspection of aged existing requires proper chemo-mechanical modeling of the combined degradation phenomena to evaluate the tolerance and to predict the remaining service life.

This thesis is focused, in particular, on the degradation process related to the sulfate attack coupled with freeze-thaw damage. The sulfate attack in concrete consists of a complex set of reactions between sulfate ions and calcium aluminates present in the cement paste. The final product of these reactions is the secondary ettringite that generates tensile stresses inside the material. On the other hand, frozen water (ice), having 9% more volume compared to water, also exerts tensile stresses on the pore walls. Microcracks get nucleated when these tensile stresses exceed the tensile strength of concrete. These microcracks increase the porosity of the concrete. This allows more water and expansive products in concrete inducing more tensile stress and damage. These complex interactions result in a highly nonlinear coupled problem that needs to be investigated from a fundamental understanding. When a concrete structure is situated in a geological site that is naturally rich in sulfates and undergoes freeze-thaw cycles the phenomena of sulfate attack coupled with freeze-thaw damage cannot be circumvented. There is no available solution to prevent this problem, but to mitigate the mechanical consequences of these detrimental effects. To fully understand this complex phenomenon, the present work aims to develop a constitutive model that can simulate the mechanical effects related to the delayed formation of ettringite that is further damaged due to freeze-thaw attacks.

Research objective

While there has been numerous work in the development of physio-chemical degradation of concrete, modeling of coupled environmental degradation modes is still in its infancy. Observation of the coupled damage process due to either SA or F-T to date has been conducted using experimental methods. However, these experimental methods are extremely time-consuming and require continuous monitoring. Furthermore, there is no

published work elucidating the combined effects of SA and F-T. Validated mathematical models, on the other hand, are powerful tools to predict the degree of deterioration with minimal error. The objective of this research work is to develop such mathematical models to assist future research endeavors with theoretical understanding.

This thesis is a compilation of two such theoretical models. One of them predicts sulfate induced damage in an unsaturated cementitious medium. A comprehensive survey of literature revealed that there is a lack of sulfate diffusion model that varies with ambient temperature. Hence, the first model is developed to describe a sulfate diffusion model that takes the current moisture content and temperature to simulate sulfate induced damage in concrete.

Freeze-Thaw damage of concrete, on the other hand, is predominant in geographical regions having temperature fluctuations around freezing temperature of water. Some of these regions contain sulfate species in soils and interact with the damage mechanism of SA. Although, several experimental investigations were conducted to capture damage induced by the combined effect of SA and F-T (Jiang, Niu, Yuan, & Fei, 2015, Y. Li, Wang, Li, Zhao, & Qin, 2018, Piasta et al., 2015), these phenomenological observations cannot serve as a theoretical basis to land on physical understanding. No mathematical models have been developed to date. Therefore, the second model, combines the SA model explained in the first manuscript with the classical theory of freezing and simulates the coupled degradation due to the combined effect of SA and F-T.

Outline of this thesis

This thesis is structured in three following chapters.

Chapter 2 is dedicated to the presentation of the first manuscript (published in ASCE Journal of Engineering Mechanics) that deals with the development of a sulfate diffusion model in an unsaturated medium.

Chapter 3 presents the second manuscript that exploits the developed model in manuscript one and shows the development of a freeze-thaw model of concrete. Finally, this chapter shows the damage incurred by concrete due to coupled freeze-thaw and sulfate attack.

Chapter 4 is devoted to the discussion of the results of the developed models. The conclusion of this pioneering work is also presented.

REFERENCES

- Jiang, L., Niu, D., Yuan, L., & Fei, Q. (2015). Durability of concrete under sulfate attack exposed to freeze-thaw cycles. *Cold Regions Science and Technology*, 112, 112–117. <https://doi.org/10.1016/j.coldregions.2014.12.006>
- Li, Y., Wang, R., Li, S., Zhao, Y., & Qin, Y. (2018). Resistance of recycled aggregate concrete containing low- and high-volume fly ash against the combined action of freeze–thaw cycles and sulfate attack. *Construction and Building Materials*, 166, 23–34. <https://doi.org/10.1016/j.conbuildmat.2018.01.084>
- Piasta, W., Marczewska, J., & Jaworska, M. (2015). Durability of air entrained cement mortars under combined sulphate and freeze-thaw attack. *Procedia Engineering*, 108, 55–62. <https://doi.org/10.1016/j.proeng.2015.06.119>

CHAPTER TWO: CHEMO-MECHANICAL MODELING OF SULFATE ATTACK-
INDUCED DAMAGE PROCESS IN CEMENT STABILIZED PAVEMENTS¹

Abstract

Cement stabilized pavement layers are subject to Sulfate Attack (SA) in sulfate abundant regions due to the internal expansion-induced damage throughout its expected service life. SA is a coupled physical-chemical-mechanical damaging process for cementitious materials involving complicated chemical reactions between sulfate and components of cement composite. SA contains intricate interactions between porous media, moisture transport, and heat transfer. Engineering mechanics has been employed to explain the failure process of the internal expansion caused by this coupled physical-chemical ingress phenomena. Existing studies have considered only heat transfer or moisture content dependent modeling. It lacks a comprehensive model that considers coupled interaction of temperature and humidity upon sulfate ingress. Thus, we developed a chemo-mechanical (CM) model for capturing the true failure process of cement stabilized pavement subgrade under SA. In this paper, a set of governing equations are developed and a unique expression for moisture and heat dependent sulfate diffusion coefficient is proposed. Consequently, the equations are solved using the finite element method. The results conform well to the experimental results. The model has been validated to be accurate enough compared to the previously implemented models. It is capable of

¹ With permission from ASCE

evaluating and predicting SA induced expansive failure in unsaturated cement stabilized pavements. Two different models were combined to estimate the mechanical behavior of cement stabilized subgrades subject to SA. Finally, Drucker-Prager (DP) failure criterion was employed for determining the damage zone.

Author keywords: Concrete; Unsaturated media; Sulfate attack; Deterioration; Evaluation.

Introduction

Pavements constructed over expansive soils are critically affected by vertical deformations of the supporting subgrade soils. Significant volume change occurs when expansive clay soils experience deviation in moisture content in the surrounding environment. Expansive soils are deleterious to the pavements because they produce unwanted tensile stress in the roads. As a result, it produces unwanted bumps and dips that make the ride uncomfortable. From the available remedial methods for this swelling problem, stabilization additives are relatively easy. Some of the additives for stabilizing expansive subgrade include lime, cement, fly ash, industrial waste products, potassium nitrate, calcium chloride and phosphoric acid (Croft, 1967). Cement, a low cost but effective additive, is widely used in the pavement industry to enhance the mechanical properties of the subgrade. In this work, we developed a coupled chemo-mechanical model to predict the mechanical performance of the cement stabilized subgrades and degradation of this stabilized layer due to SA.

It is expected that cement stabilized layers support the traffic loads by maintaining a lower swelling potential throughout its expected service life. However, cementitious materials subjected to environmental ingresses lose mechanical stability and durability due

to several factors. For example, moisture and heat transport weakens the microstructure of cementitious materials, freeze-thaw phenomenon nucleates microcracks by inducing thermal stress (Jacobsen & Sellevold, 1996), sulfate attack, carbonation or the chloride intrusion are responsible for the volume expansion, resulting in damage in the cementitious material (Cefis & Comi, 2017). SA in cementitious materials is the focus of this work. Cementitious materials under hydration produce expansive ettringite when sulfation of alumina takes place in cement stabilized subgrade layers. In order to predict the damage of stabilized subgrade due to SA in field conditions, a model is desirable to consider field conditions, i.e. variable temperature and unsaturated sample. In this paper, we attempted to model the SA coupled with temperature and moisture distribution.

SA in cement stabilized subgrade follows a complex set of reactions between sulfate ions and the hydrated calcium aluminates (C_3A , C_4AF) in the cement paste. Sulfate ion (SO_4^{2-}) in cementitious materials may emanate from two sources and depending on the source the SA process can be divided into two types. When sulfate ion penetrates inside cementitious material from outside, this is termed as *External Sulfate Attack* (ESA). Alternatively, when it is nucleated inside due to high heating, it is called the *Internal Sulfate Attack* (ISA). ISA is also termed as *Delayed Ettringite Formation* (DEF) (Skalny et al., 2001) or secondary ettringite to differentiate it from the initial ettringite formation (Fu et al., 1994). Cement stabilized subgrades undergo damage regardless of the method of sulfate ingress inside the cementitious materials. Furthermore, two types of damage can occur by SA: loss of mechanical strength due to C-S-H degradation and volume expansion causing micro cracks (Tixiër & Mobasher, 2003). Experimental evaluation of this coupled chemical degradation phenomena is very difficult. It is almost impossible to measure those

critical properties from an experimental setup, especially at the interface or pore scales. Therefore, a reliable model is necessary to predict the service life of cement stabilized pavements imperiled to sulfate attack.

Many researchers have attempted to model the sulfate attack and corresponding mechanical damage to cementitious materials (Bary, 2008, Basista & Weglewski, 2008, Basista & Weglewski, 2009, Sarkar et al., 2010, Cefis & Comi, 2017). A simplified chemo-mechanical model of ESA was proposed by Bary (Bary, 2008). In this model, the author assumed that the cement stabilized layer is fully saturated and placed in an isothermal environment. It was further assumed that the calcium concentration in pore solution is adequate to define the mechanical degradation state. Volume expansion due to SA was modeled by Clifton (Clifton & Pommersheim, 1994). However, the model was autonomous to the condition of the current reactants and reaction products, which leads to the computation of unrealistic volume expansion. This ambiguity was taken into account the model proposed by Basista (Basista & Weglewski, 2009). This model solves the unsteady diffusive transport equation coupled with reaction kinetics equations to compute the spatial and temporal distribution of sulfate ions. Finally, the volume expansion can be calculated as eigenstrain. Note that the strain that occurs due to physical changes, i.e. thermal expansion, expansion due to chemical reaction, without the involvement of any external load is called eigenstrain. The authors also assumed an initially saturated sample to avoid solving the moisture transport equation. In addition, the concentration gradient of sulfate inside cementitious material controls the transport of sulfate ions inside the domain.

Along with the dependence of moisture transport, SA also depends on temperature distribution. Some experimental attempts have been conducted to investigate the effect of

temperature variation on the sulfate attack. Ping (Ping & Beaudoin, 1992) has endeavored to study the effect of temperature change on SA. They laid a thermodynamic framework for detection of sulfate related expansion and found that expansion was proportional to the temperature of the sulfate solution. The major effect of temperature is a rise in crystallization pressure as a result of the solid product formation, which corroborates the deduction made by Lawrence (Lawrence, 1990). Findings from this research suggested that increasing the temperature will reduce the time required to get to the objective expansion. In other words, the rise in temperature will accelerate the rate of SA.

Research Objective

The significant limitations of all the discussed models in the introduction were that they either considered a saturated sample for the model or isothermal condition was assumed. The objective of this work is to achieve a better understanding of SA in complex sulfate environments by developing an improved mathematical model. We investigate the dependence of SA on temperature and degree of saturation. To keep the model from getting too complex, it is assumed that the chemical reactions do not contribute to the heat generation or dissipation in the domain. It is further assumed that the water is inert and does not participate in the chemical reaction. This assumption is based on the fact that water works as a solvent and in most of the compounds in cement reaction water is consumed as a hydrate. The water being inert is an acceptable assumption and validated by Cefis and Comi (Cefis & Comi, 2017). In this work, we developed a chemo-mechanical model to predict the mechanical performance of the cement stabilized subgrades and degradation of this stabilized layer due to SA.

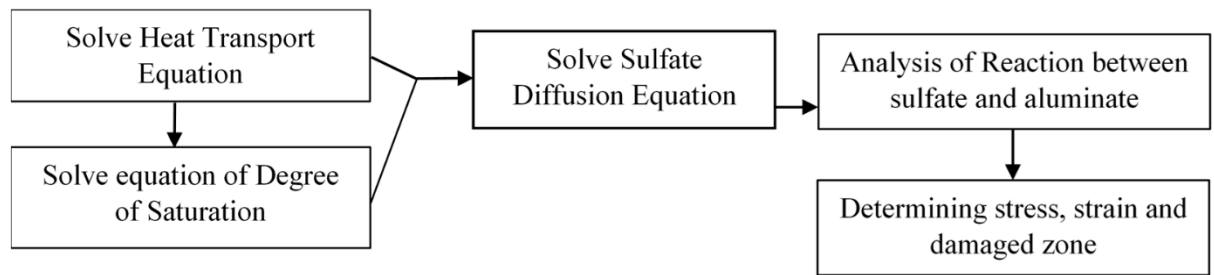


Figure 2-1. Flow diagram of the solution procedure of the proposed model

Figure 2-1 shows the step by step procedure for solving sulfate ingress. Initially, the heat transfer equation is solved to obtain the temperature gradient inside cement stabilized subgrade. To do this, we developed an equation that can take care of the heat transfer inside the unsaturated media. After that, the degree of saturation is computed using a moisture diffusion model. For moisture transport equations we need viscosity of the porous fluid. A temperature dependent viscosity is considered for this case. Therefore, moisture transport is coupled with heat transfer equation. Previously, the sulfate diffusion coefficient was determined from saturated samples of cement composite. In this work, we developed a unique expression for this diffusion coefficient that can handle unsaturated samples which lies in a non-isothermal environment. Then, using the gradient of temperature and moisture content, the solution of sulfate diffusion equation was sought along with its reaction with aluminates. Finally, the mechanical properties, i.e, eigenstrain, stress and DP function are applied to determine the damaged location.

Chemo-mechanical Mechanisms of Sulfate Attack

SA depends on many factors, including the concentration of sulfate in the solution, temperature, and humidity variations. The existing modeling framework is not able to cover SA considering unsaturated samples placed in a non-isothermal environment. This is because almost all the models are based on tests made in the laboratory, under controlled

environmental conditions. However, the behavior of cement stabilized subgrades on site in different climate regions is never the same. There will be a fluctuation of temperature and humidity that control the rate of SA in the cement stabilized subgrade. Consequently, the models lack accuracy while predicting actual sulfate ingress in field conditions. Thus, it is critical to couple these effects into a model that is developed to predict the performance of cementitious materials.

SA takes place when calcium, alumina, and sulfate are combined to form ettringite ($3CaO \cdot Al_2O_3 \cdot 3CaSO_4 \cdot 32H_2O$). The volume of ettringite is about twice the volume of the original constituents (Rollings et al., 1999), which results in excessive swelling and cracking when sufficient ettringite forms. Thus, SA in cement stabilized pavements can be mitigated by using cements containing less C3A in order to limit the supply of alumina. Usually, sulfate anion (SO_4^{2-}) comes from sodium sulfate (Na_2SO_4) solution and reacts with portlandite (CH) or Calcium-Silicate-Hydrate ($C - S - H$) gel to precipitate gypsum ($C\hat{S}H_2$) (Skalny et al., 2001), as shown in Equation 2-1.



Here, H is H_2O , \hat{S} is SO_3 , C is CaO . Following the formation of gypsum, a set of reactions takes place to form secondary ettringite. This reaction needs several steps to get completed (Cefis & Comi, 2017, Tixiër & Mobasher, 2003). Mathematical derivation details of the chemo-mechanical model development are discussed in the following sections of this paper.

Mass Balance

According to Cefis (Cefis & Comi, 2017) mass balance of an SA is a diffusion-reaction problem. The variation of concentration (c) in time depends on the divergence of

flow of moles and decay or accumulation of reactant. The relation can be described by the following partial differential equation (PDE), shown in Equation 2-2.

$$\frac{dc}{dt} = -\nabla \cdot \tilde{f} + \zeta \quad (2-2)$$

here ∇ is a differential operator and is given by $\nabla = \frac{\partial}{\partial x} \tilde{i} + \frac{\partial}{\partial y} \tilde{j} + \frac{\partial}{\partial z} \tilde{k}$, here $\tilde{i}, \tilde{j}, \tilde{k}$ are unit vectors in x, y and z directions respectively. \tilde{f} is the flow of moles and ζ is the source or sink of reactant. A positive value of ζ indicates a source and a negative value means a sink.

The flow of moles can be defined as the flux of reactant \tilde{M} per unit molar volume v_m .

$$\tilde{f} = \frac{\tilde{M}}{v_m} \quad (2-3)$$

where molar volume is related to molar mass (M_m) and intrinsic density ρ by $v_m = \frac{M_m}{\rho}$, so, Equation 2-3 can be rewritten as,

$$\tilde{f} = \frac{\rho \tilde{M}}{M_m} \quad (2-4)$$

A compact form ettringite formation can be given by Equation 2-5 (Tixier & Mobasher, 2003).



where C_a is the equivalent grouping of calcium aluminates participating in the reaction and is given by $C_a = \sum_{i=1}^m \gamma_i P_{ri}$ and q is the stoichiometric coefficient of reaction defined by $q = \sum_{i=1}^m \gamma_i a_i$. Here, m is an integer; diverse values were adopted by different researchers for m . It indicates how much aluminate components is considered that participate in the chemical reaction. Tixiër (Tixiër & Mobasher, 2003) used a value of 3,

whereas Cefis (Cefis & Comi, 2017) used 4 for the same quantity. Here, γ_i represents the proportion of aluminate represented by P_{ri} (reacting calcium aluminate) and $\sum_{i=1}^m \gamma_i = 1$. Both authors declared C_4AH_{13} , $C_4A\hat{S}H_{13}$ and C_3A as i th component of P_r . However, Cefis included C_4AF with the previous ones. Finally, r indicates the stoichiometric weighting coefficient of water.

The equations for simulating the chemical reaction of SA in saturated isothermal condition reported by Cefis (Cefis & Comi, 2017) is as follows,

$$\frac{d[CA]}{dt} = -\frac{k}{q} [CA][S] \quad (2-6)$$

$$\frac{d[S]}{dt} = \nabla \cdot (D_s \nabla [S]) - k[CA][S] \quad (2-7)$$

Here $[CA]$ and $[S]$ denotes the concentration of calcium aluminate and sulfate, respectively. k is the rate constant and D_s is the diffusion coefficient of sulfate in saturated concrete. The negative sign in Equation 2-6 signifies that as the reaction progresses the concentration of calcium aluminate and sulfate depletes.

Sulfate Attack in Unsaturated Sample

After a brief explanation of the SA mechanism and mass balance process, now we can proceed with the model development. Previously almost all the models could describe SA in the saturated sample. However, cement stabilized subgrades do not always remain in saturated condition. To imitate the reality, a model is required that can handle “unsaturated sample”. Cefis (Cefis & Comi, 2017) proposed a weakly coupled approach based on the framework of porous material (Coussy, 2004). This model is capable of solving degree of Saturation, S_w , using a nonlinear diffusion equation provided in Equations 2-8 and 2-9.

$$\phi \frac{\partial S_w}{\partial t} = \nabla \cdot (D_w \nabla S_w) \quad (2-8)$$

$$D_w = \frac{dp_c}{dS_w} \frac{\kappa}{\eta_w} \sqrt{S_w} \left(1 - \left(1 - S_w^\beta \right)^{\frac{1}{\beta}} \right)^2 \quad (2-9)$$

Here, ϕ is porosity, D_w is water diffusion coefficient, p_c is capillary pressure, κ is intrinsic permeability, η_w is dynamic viscosity given by $1.38 \times 10^{-6} e^{-\frac{2590}{T}}$ with T being absolute temperature, and β is a material parameter comes from the relationship between capillary pressure and degree of saturation.

$$p_c = \alpha \left(S_w^{-\beta} - 1 \right)^{1-\frac{1}{\beta}} \quad (2-10)$$

The values of α and β were found to be 11.2 and 2.84 respectively by fitting experimental data points. Therefore, Equations 2-9 and 2-10 becomes,

$$D_w = -\frac{20.68 S_w^{-3.84}}{(S_w^{-2.84} - 1)^{0.35}} \frac{\kappa}{\eta_w} \sqrt{S_w} \left(1 - \left(1 - S_w^{2.84} \right)^{0.35} \right)^2 \quad (2-11)$$

$$p_c = 11.2 (S_w^{-2.84} - 1)^{0.65} \quad (2-12)$$

Usually, the boundary condition (BC) for solving the degree of saturation comes from relative humidity (RH) (Cefis & Comi, 2017). RH is defined as the ratio of existing vapor pressure to the saturated vapor pressure at the same temperature. Capillary pressure as a function of RH is given by $p_c = -\rho_w \frac{RT}{m_v} \ln(RH)$. Replacing this expression of p_c in Equation 2-12 forms the BC written as Equation 2-13. The following BC along with Equations 2-8 and 2-11 yield the distribution of the degree of saturation.

$$S_{wb} = \left[\left(-\rho_w \frac{RT}{11.2 m_v} \ln(RH) \right)^{1.538} + 1 \right]^{-0.352} \quad (2-13)$$

where m_v is the mass of one mole of water vapor, R is universal gas constant, T is absolute temperature and ρ_w is the water density. S_{wb} denotes the constant degree of saturation on the boundary. It is applied on the potential boundary through which flow of moisture takes place.

The diffusion of sulfate ions is determined by the gradient of sulfate concentration and moisture content inside the cement stabilized subgrade media. We use the equations proposed by Cefis (Cefis & Comi, 2017) for sulfate ingress and reaction with aluminate phase to model the unsaturated conditions, as given by the following equations:

$$\frac{d[CA]}{dt} = -\frac{k}{q}[CA][S] \quad (2-14)$$

$$\frac{d[S]}{dt} = \nabla \cdot \left\{ D'_s S_w \nabla \left(\frac{[S]}{S_w} \right) \right\} + D_w \frac{[S]}{S_w} \nabla S_w - k[CA][S] \quad (2-15)$$

Here, D'_s indicated the isothermal diffusion coefficient of sulfate ion in unsaturated medium and is given by (Samson, et al., 2005)

$$D'_s = D_s \sqrt[3]{S_w} \quad (2-16)$$

where, D_s is the sulfate diffusion coefficient in fully saturated cement stabilized subgrade, S_w is the degree of saturation.

Effect of Heat on Sulfate Attack

In addition to moisture effects, Condor (Condor et al., 2011) showed that sulfate diffusion depends on temperature as well. Using the data points provided by them, a figure is drawn which is shown in Figure 2-2.

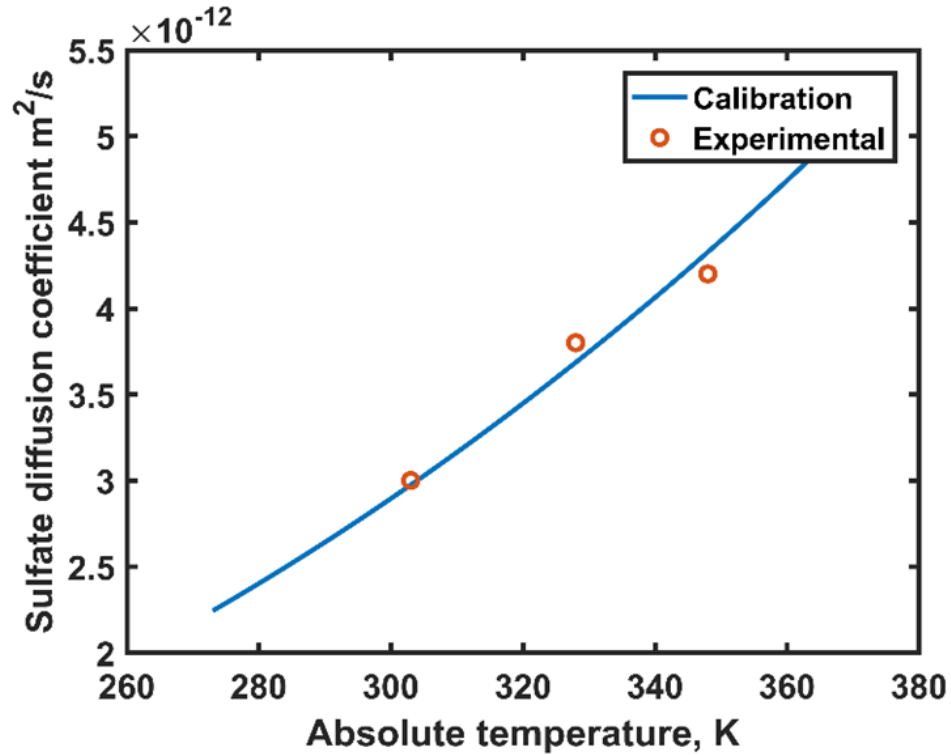


Figure 2-2. Variation of sulfate diffusion coefficient with temperature

A power model ax^b can be used to describe this behavior, and the following relation is derived by describing diffusion coefficient as a function of absolute temperature, T .

$$D_s = 5.736 \times 10^{-19} T^{2.706} \quad (2-17)$$

Note that D_s given in Equation 2-17 gives the variation of sulfate diffusion coefficient at different temperatures. However, this relation is valid for saturated samples only. We need to modify this equation to determine the sulfate diffusion in unsaturated and non-isothermal condition.

Putting D_s from Equation 2-17 into Equation 2-16, for the first time we created a diffusion coefficient for unsaturated and non-isothermal condition, as shown in Equation 2-18.

$$D_s'' = 5.736 \times 10^{-19} T^{2.706} \sqrt[3]{S_w} \quad (2-18)$$

Note that this equation innovatively includes the unsaturation factor into the determination of non-isothermal diffusion coefficient (D_s'') of sulfate ion in unsaturated medium. We developed Equation 2-18 so that the sulfate diffusion coefficient (in m^2/s) can be determined based on the unsaturated and non-isothermal conditions. In previous models or experimental works, sulfate diffusion coefficient was only reliant on degree of saturation (Cefis & Comi, 2017) or on temperature (Condor et al., 2011). Figure 2-3 is plotted using the newly developed Equation 2-18 showing the variation of diffusion coefficient of sulfate ingress with temperature and degree of saturation.

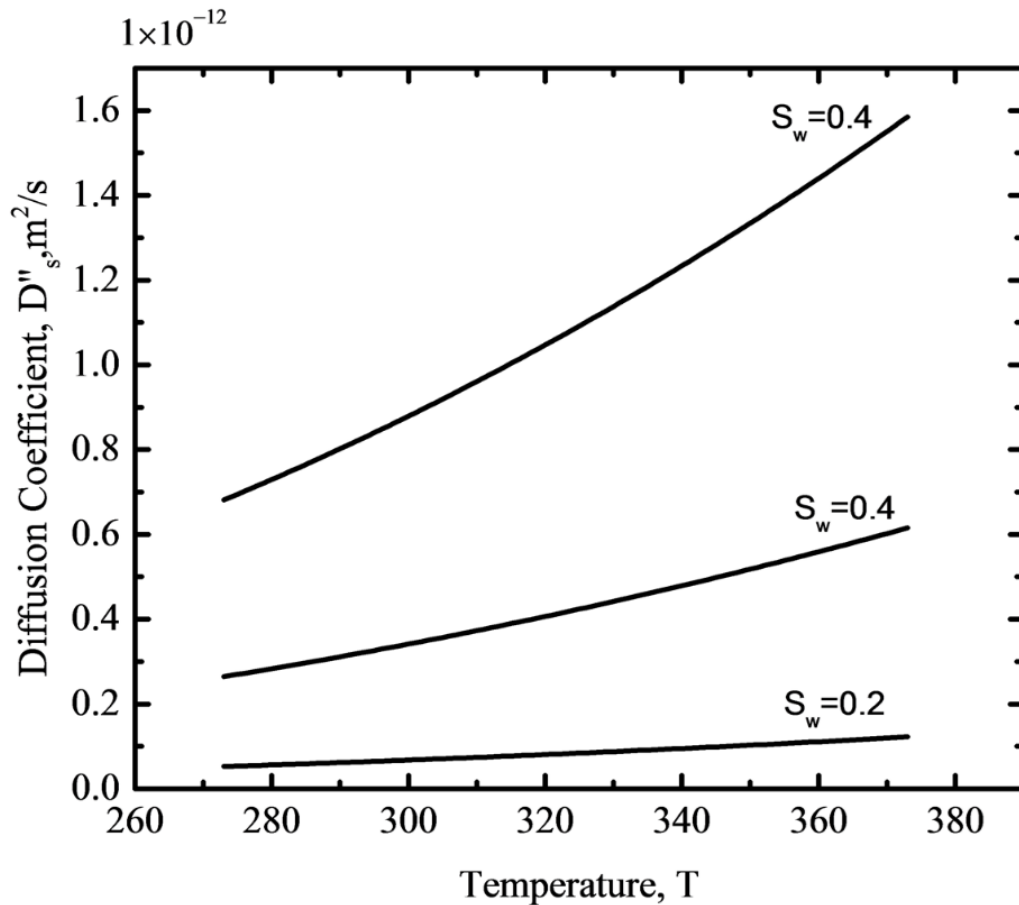


Figure 2-3. Variation of sulfate diffusion coefficient

Figure 2-3 explains how the coefficient of sulfate diffusion changes with temperature and degree of saturation. For example, at a saturation degree of 0.4 and a temperature of 273 K, the sulfate diffusion coefficient is 2.64×10^{-13} . For the same temperature and a higher degree of saturation of 0.6, the diffusion coefficient increases to 6.82×10^{-13} . This indicates a 158% increase in diffusion coefficient compared to the 50% increase in the degree of saturation. Now at an elevated temperature of 373 K and the degree of saturation of 0.6, the diffusion coefficient becomes 1.58×10^{-12} marking an increase of 131%. However, for a different degree of saturation (i.e. 0.4), this coefficient increases from 2.64×10^{-13} to 6.16×10^{-13} (133% increase) under the temperature change from 273.15 K to 373.15 K. Therefore, it is apparent that for a sample with a constant degree of saturation the sulfate diffusion coefficient increases with temperature. This supports the fact that higher temperatures result in higher diffusion/migration coefficients (Yuan et al., 2009). However, as seen from the analysis, the rate of change of diffusion coefficient with temperature is different for a different degree of saturation. The maximum possible value of S_w can be 1 indicating a fully-saturated sample. At full saturation, the diffusion coefficient given by Equations 2-18 and 2-17 will necessarily be the same.

Heat Transport in Cement Stabilized Subgrade

As we can see, the created model requires temperature and saturation degree as an input for Equation 2-17 to obtain the diffusion coefficient. We need to solve the heat transfer equation to estimate the distribution of heat inside the cementitious material. Heat transport inside cement stabilized subgrade is modeled based on the framework of heat transfer through porous media presented by Nield (Nield and Bejan, 2017). This model was based

on the assumption that cement composites have two phases; solid and porous structure. In this work, we use Nield's framework of heat transfer through porous media. The heat transfer through a porous medium is given by,

$$(1 - \phi)\rho_s c_s \frac{\partial T_s}{\partial t} = (1 - \phi)\nabla \cdot (k_s \nabla T_s) + (1 - \phi)q_s \quad (2-19)$$

and through the fluid phase, it is given by,

$$\phi \rho_f c_f \frac{\partial T_f}{\partial t} + \rho_f c_{pf} \tilde{v} \cdot \nabla T_f = \phi \nabla \cdot (k_f \nabla T_f) + \phi q_f \quad (2-20)$$

here, the subscripts s and f denotes solid and fluid phase. ρ is density, c is specific heat, c_p is specific heat at constant pressure of the fluid, k is thermal conductivity, and q_s and q_f are source terms for diffusing heat through solid and porous fluid. A positive value of this quantity means addition of heat inside the domain, a negative value means withdrawal of the same. \tilde{v} denotes the velocity of the fluid flow through a porous medium.

In this CM model, porosity (ϕ), was computed using Powers model which states that porosity of cementitious materials is a function of degree of hydration (ω), water cement ratio (w/c) and proportion of cement in the mix (V_c) (Hoglund, 1992), which is given by,

$$\phi = V_c \frac{\frac{w}{c} - 0.39\omega}{\frac{w}{c} + 0.32} (> 0) \quad (2-21)$$

Similar to other models, the heat transfer model depicted by Equations 2-19 and 2-20 also assume saturated medium for simplicity of model development. Hence, we need to make some adjustment to extend its capability to handle unsaturated medium as well. A novel term ϕ_f is considered for a fraction of pores that are filled with water. This quantity can be calculated by multiplying porosity with the average degree of saturation over the

entire volume of the model. Average degree of saturation may be computed by smearing the quantity throughout the volume,

$$\bar{S}_w = \frac{1}{v} \int_0^v S_w dv \quad (2-22)$$

Here, v is the volume of the domain. Thus ϕ_f can be computed by using the following equation,

$$\phi_f = \phi \bar{S}_w \quad (2-23)$$

Replacing ϕ with ϕ_f in Equation 2-20, we get

$$\phi_f \rho_f c_f \frac{\partial T_f}{\partial t} + \rho_f c_{pf} \tilde{v} \cdot \nabla T_f = \phi_f \nabla \cdot (k_f \nabla T_f) + \phi_f q_f \quad (2-24)$$

We modified Equation 2-20 to develop Equation 2-24 for enhancing the capability of the heat transfer model. After this augmentation, the heat transfer model, given by Equations 2-19 and 2-24, is now capable of considering the heat transfer in unsaturated or partially saturated cement stabilized subgrade sample. Please note that, Equations 2-19 and 2-24 simulates heat transfer through solid media and porous fluid respectively. These equations may produce quasi-static heat distribution in a macro-level or a continuum level model due to low rate of flow. However, differential heat distribution may be observed during analyzing a model containing microstructure. Hence, a two-phase heat migration model is considered in this model. Also note that, Equation 2-23 needs to be further studied to validate the relation between partially saturated porosity and an average degree of saturation. In following sections of the paper, a compacted form of the model depicted by Equations 2-8 to 2-24 is presented.

Governing Equations for Coupled CM Behavior Under SA

Sulfate attack in cementitious materials is a complicated mechanical damage process governed by the coupled chemical reaction, thermal, and moisture transport effects. Previous models assumed several factors to keep the complexity at a manageable level. However, the tradeoff was compromising the accuracy of the model. In order to improve the model accuracy, thermal effect on SA is included in the equation to account diffusion coefficient for sulfate ingress. This resulted in a coupled PDE set that explains the interaction and interplay of moisture transport, heat transfer, and sulfate attack and sulfate-aluminate reaction. The governing equation consists of a set of five equations that are coupled together by their dependent variables. The constitutive equation is provided in Equation 2-25,

$$\left\{ \begin{array}{l} \phi \frac{\partial S_w}{\partial t} = \nabla \cdot (D_w \nabla S_w) \\ \frac{d[S]}{dt} = \nabla \cdot \left\{ D_s'' S_w \nabla \left(\frac{[S]}{S_w} \right) \right\} + D_w \frac{[S]}{S_w} \nabla S_w - k[CA][S] \\ \frac{d[CA]}{dt} = -\frac{k}{q}[CA][S] \\ (1 - \phi) \rho_s c_s \frac{\partial T_s}{\partial t} = (1 - \phi) \nabla \cdot (k_s \nabla T_s) + (1 - \phi) q_s \\ \phi_f \rho_f c_f \frac{\partial T_f}{\partial t} + \rho_f c_{pf} \tilde{v} \cdot \nabla T_f = \phi_f \nabla \cdot (k_f \nabla T_f) + \phi_f q_f \end{array} \right. \quad (2-25)$$

Equation 2-25 consists of the governing equations for the coupled CM behavior of sulfate attack in cement stabilized subgrades. The first equation gives the distribution of the degree of saturation. In this equation moisture diffusion coefficient (D_w) is dependent on temperature through temperature dependent dynamic viscosity of water. The second equation describes the sulfate diffusion inside cementitious materials. This equation is coupled in a complex way with both temperature (through diffusion coefficient, D'') and

saturation degree (S_w) of the stabilized subgrade sample. The third equation explains sulfation of aluminate. Finally, the fourth and fifth equation explains the heat transfer in an un-saturated medium.

Matlab Partial Differential Equation (PDE) Toolbox™ has been used to solve the coupled set of equations shown in Equation 2-25. This PDE Toolbox™ provides functions for solving partial differential equations (PDEs) in 2-D, 3-D using finite element analysis. Both static and transient problems can be solved using Matlab PDE solver.

Mechanical Damage due to Sulfate Attack

The constitutive equation given by Equation 2-25 can model the SA in unsaturated concrete under non-isothermal condition. For engineering purposes, we want to predict the potential damage due to SA-induced internal expansion. The internal expansion causes tensile stress within the cementitious porous media. The growth of tensile stress nucleates the formation of micro-cracking (mechanical damage) and follow up with crack propagation and failure process. In this section, we concentrate on developing the mechanical damage model. Recently, in a laboratory test piloted by Santhanam (Santhanam et al., 2002) found that expansion rate due to SA increases with time. To take into account the change in the rate of expansion with time in a simplified way they divided the profile into two stages. This differentiation appears at a critical time, t_c , shown in Figure 2-4.

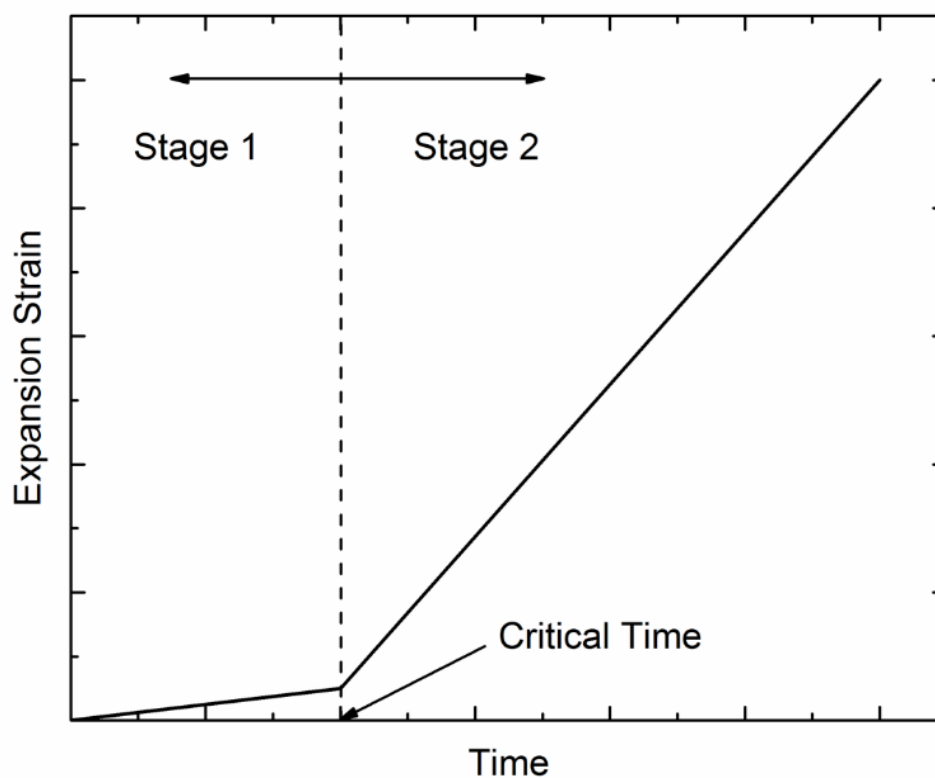


Figure 2-4. Qualitative diagram of variation of expansion strain with time

Stage 1 prevails until this critical time (estimated using Equation 2-28) and after this time have passed stage 2 takes over. The rate of volume change is less steep in stage 1 than stage 2 demonstrating a higher expansion rate at stage 2. They also concluded that the concentration of sulfate solution has an effect on the second stage of the volumetric strain rate. The increase in sulfate concentration accelerates the rate of change of volume causing the second stage curve steeper.

Santhanam (Santhanam et al., 2002) developed a concentration model to represent the first stage by,

Rate of expansion

$$= 3.74 \quad (2-26)$$

$$\times 10^{-10} (\text{Concentration of } SO_3, \text{ in mol/l } Na_2SO_4)^{0.89} \%/\text{week}$$

The second stage of SA starts after the critical time, t_c , and the activation energy is calculated to estimate the termination time of the first stage. The Arrhenius relation (Laidler, 1984) can be used to determine the activation energy and is given by,

$$k = Ae^{\frac{-E_a}{RT}} \quad (2-27)$$

where A is the frequency factor that explains the interatomic collision, and E_a is activation energy and for Na_2SO_4 this is estimated to be 8861.4 cal/mol . The time taken to complete stage 1 is reciprocal of the reaction rate constant, k , and is reported as Equation 2-28. As we can see, the reaction rate constant, k , is dependent on absolute temperature T . This equation couples the sulfate attack reaction with heat transfer.

$$t_c = e^{\left(\frac{4430.7}{T} - 11.45\right)} \quad (2-28)$$

Equation 2-28 gives the critical time after which stage 2 starts. A visualization of critical time is given in Figure 2-4. This model is limited to determine the strain of cementitious materials after critical time has passed. Thus, the damage model estimates the concrete damage when the cementitious material is at stage 2 of SA.

The expansive strain due to SA is approximated using Equation 2-26. This equation gives the percentage of expansion per week. Then, using the sulfate concentration inside cementitious materials, we can estimate the expansion using Equation 2-26. Consequently, the eigenstrain can then be estimated using this value by the following equation,

$$\epsilon = \frac{\Delta V}{V} \quad (2-29)$$

here, ΔV is the volumetric expansion calculated using Equation 2-26 and V is the initial volume. Please note that, Equation 2-26 calculates the rate of expansion or volume

change per week. Multiplying elapsed time with this quantity will produce the volume change accumulated in the specified time.

Finally, stress is calculated using the constitutive equation given by Equation 2-30.

$$\sigma = E\epsilon \quad (2-30)$$

As the ettringite crystal grows under sulfate attack, the expansion stress and strain gradually increase. To estimate the mechanical failure, we evaluate pavement subgrade failure using Drucker-Prager (DP) (Drucker & Prager, 1952) yield criterion. The DP yield criterion is a stress-dependent model given by Equation 2-30. It has been accepted to determine whether a stone-based material has failed or undergone plastic yielding. Note that the concrete specimen undergoes three-dimensional complex stress status until the mechanical failure mode occurs. The DP model can capture the behavior of concrete and determine the onset of concrete failure behavior. Furthermore, Jose (José & Cela, 1998) reported that the DP model is capable of predicting the accumulation of plastic strain located in tensile zones. Hence, DP yield criterion is used to determine the yielded part of concrete due to tensile stress. This model is subject to further development, and in the future release a more efficient model capable of capturing damage due to fracture will be incorporated. DP yield criterion is given in Equation 2-31.

$$\begin{cases} \sqrt{J_2} - A + BI_1 = 0 \\ A = \frac{2}{\sqrt{3}} \left(\frac{\sigma_c \sigma_t}{\sigma_c + \sigma_t} \right) \\ B = \frac{1}{\sqrt{3}} \left(\frac{\sigma_t - \sigma_c}{\sigma_c + \sigma_t} \right) \end{cases} \quad (2-31)$$

Here, J_2 is the second invariant of stress tensor, I_1 is the first invariant of stress tensor, σ_c and σ_t are the compressive strength and tensile strength of cementitious materials.

Results and Discussion

The developed governing Equation 2-25, describing sulfate ingress phenomena, is strongly convoluted and intensely coupled that analytical solutions can hardly be obtained. Hence, numerical solutions are sought by using the finite-element method implemented in an interactive environment. This numerical solution procedure is developed with a view to i) validating the proposed mathematical model by a comparison of the analytical results with available experimental data; ii) predicting the distribution of sulfate, moisture, and temperature after 400 days. The validation and application of the predictive model are described in the following sections.

Validation of the Proposed Model

A simulation scheme was set up to reproduce the experiments performed by Condor (Condor et al., 2011). They conducted an experimental investigation on the impact of temperature on the diffusion of sulfate inside concrete. A 2-D domain was used for simulating the experiment and shown in Figure 2-5.

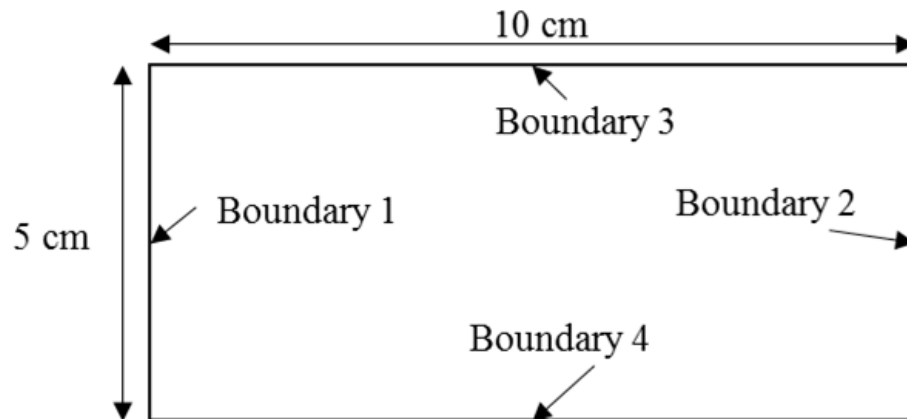


Figure 2-5. Simulation domain showing dimension and boundary numbers

The initial and boundary conditions along with parameters for simulating the experiment is provided in Table 2-1 and Table 2-2, respectively.

Table 2-1. Initial and boundary condition for the simulation

Boundary condition		Initial condition	
Boundary 1		S_w	0
RH	50%	[CA]	$82.5 \text{ mol} \cdot \text{m}^{-3}$
[CA]	0	[S]	0
[S]	$700 \text{ mol} \cdot \text{m}^{-3}$	T	293.15 K (20°C)
T	313 K (40°C)		
Boundary 2,3,4	Zero flux		

It was assumed that a constant relative humidity, concentration of substrates and temperature was maintained throughout the experiment. It was reported by Little (Little & Nair, 2009) that sulfate concentration in soil could reach up to 10,000ppm or mg/kg of soil mass. Additionally, typical soil moisture content ranges from 10 to 35% by mass. Hence, in 1 kg of soil there will be 100 to 350g of water in natural condition. As a result, 10,000mg or 10g of sodium sulfate will be dissolved in say 200g of water. Since, the density of water is $1g/cm^3$ so, 10g of sodium sulfate will be dissolved in say $200cm^3$ of water. The molar weight of sodium sulfate is $142.04g/mol$. So, 10g of sodium sulfate is equivalent to $0.071mol$. This means that $0.071mol$ of sodium sulfate is dissolved into $200cm^3$ or $0.0002m^3$. So, the molarity of the sodium sulfate in soil can reach up to $\frac{0.071}{0.002} = 355mol/m^3$. However, a sulfate concentration of $700mol/m^3$ was adopted to simulate extreme sulfate rich environment.

Table 2-2. Parameters used for the simulation

Parameter	Value	Parameter	Value
κ	$3e-14 \text{ m}^2 \cdot \text{mol}^{-1} \cdot \text{day}^{-1}$	ρ_s	$2400 \text{ kg} \cdot \text{m}^{-3}$
η_w	$1.38 \times 10^{-6} e^{\frac{2590}{T}} \text{ Pa} \cdot \text{s}$	c_s	$7500 \text{ J} \cdot \text{kg}^{-1} \cdot \text{K}^{-1}$
M_v	$18.015e-3 \text{ kg} \cdot \text{mol}^{-1}$	k_s	$0.8 \text{ W} \cdot \text{m}^{-1} \cdot \text{K}^{-1}$
R	$8.3145 \text{ J} \cdot \text{mol}^{-1} \cdot \text{K}^{-1}$	k_f	$0.591 \text{ W} \cdot \text{m}^{-1} \cdot \text{K}^{-1}$
k	$1.12e-4 \text{ m}^3 \cdot \text{mol}^{-1} \cdot \text{day}^{-1}$	c_f	$4.18 \text{ J} \cdot \text{g}^{-1} \cdot \text{K}^{-1}$
ρ_f	$1 \text{ g} \cdot \text{cm}^{-3}$	ϕ	0.3
c_{pf}	$4185.5 \text{ J} \cdot \text{kg}^{-1} \cdot \text{K}^{-1}$		

Two cases were considered for the model validation. Case 1: An isothermal condition, the temperature of the entire domain was kept at 303 K (30°C) to mimic the experimental condition described by Condor (Condor et al., 2011); Case 2: Using the solution of Equation 2-19 and 2-24, that gives the distributed temperature throughout the domain. The simulation results are shown in Figure 2-6. We compare the results from the existing model (Cefis & Comi, 2017) and our developed model in this paper.

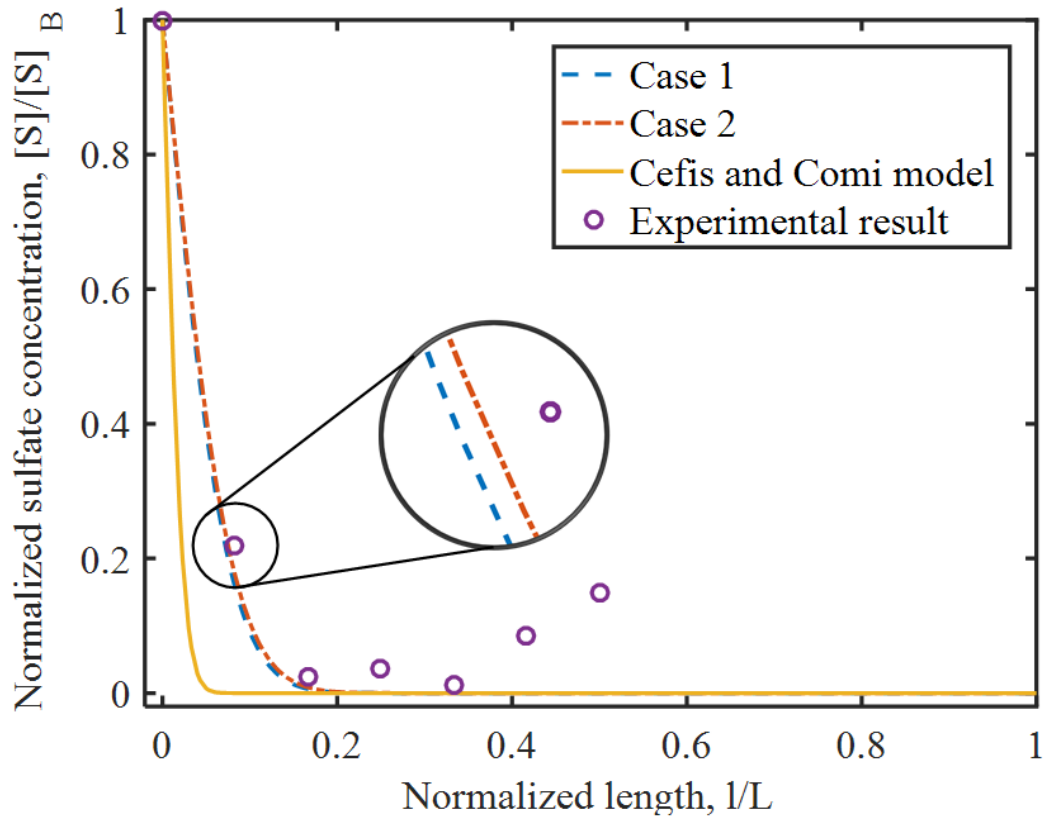


Figure 2-6. Validation of the proposed model

Figure 2-6 shows the quantity of sulfate at a normalized length of 0.1 inside cement stabilized subgrade after two months. Comparing to a normalized concentration of 0.21 in the experiment, our model predicted 0.16 for an isothermal condition and 0.18 for the non-isothermal condition. The relative error found from the simulation was 23% and 14% for isothermal and non-isothermal cases, respectively. However, Cefis model predicted 1.4×10^{-5} producing a significant discrepancy. Regression analysis showed a R^2 value of about 98% for both cases based on our model and 94% for model proposed by Cefis. Clearly, based on the analysis of the results the model proposed by Cefis (Cefis & Comi, 2017) is not reasonably accurate when it comes to the prediction of sulfate propagation front. In contrast, our model is more accurate in predicting the sulfate ingress with a slight margin

of error when the temperature is considered to be distributed evenly. Consideration of the temperature distribution slightly enhances the accuracy of the model by reducing the relative error from 23% for isothermal condition to 14% for non-isothermal condition. A close view of the plot corroborates this argument. However, a 14% error still exists, which could potentially be due to not considering PH of the solution, temperature released by the reaction in the model.

The experimental result was adopted from Condor (Condor et al., 2011) and the data points around the normalized length of 0.5 may be referred to as noises measured using the scanning electron microscope (SEM). In both of the cases, the sulfate propagation front stopped at the normalized length of 0.2 agrees with the experimental result. This shows how our model is better than the previously developed model without considering the non-isothermal condition.

Here is an analysis of the reactants amount consumed during the SA process. In our model, the reaction between sulfate and aluminates takes place as a first order reaction. This implies that the concentration of reactants will decay exponentially. The drop in aluminate concentration with time is shown in Figure 2-7 as a function of time. On the other hand, as cementitious material ages, the sulfate gets accumulated inside it. Two trends of sulfate accumulation (with and without reaction with aluminate) are plotted in Figure 2-7 along with the concentration profile of aluminate.

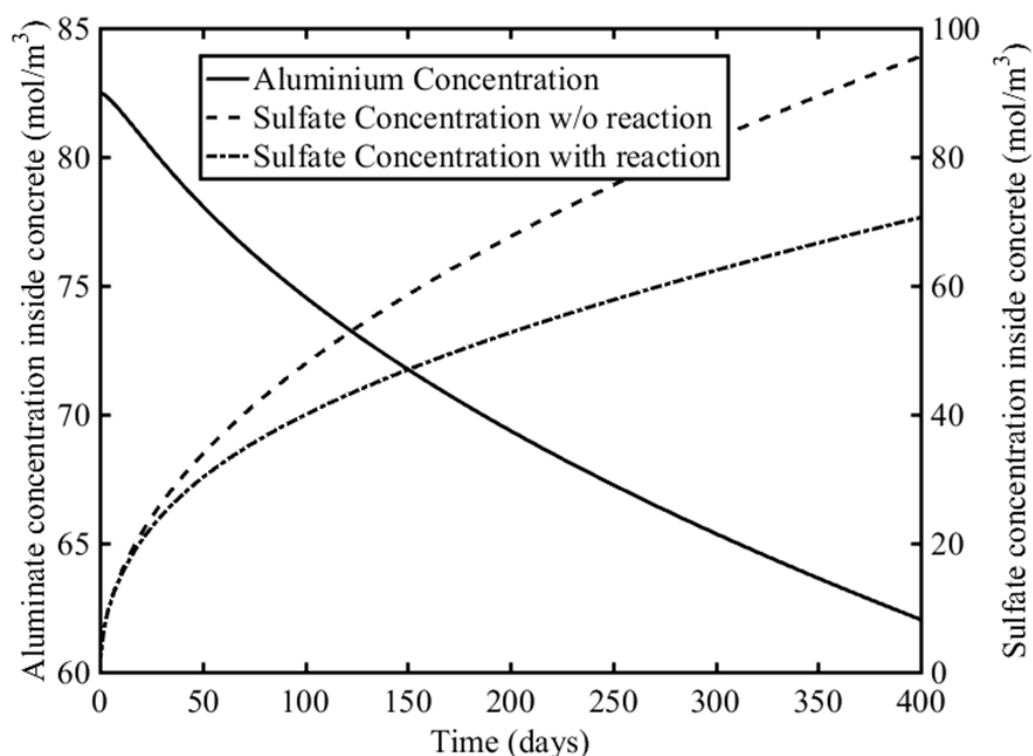


Figure 2-7. Changes in concentration of sulfate and aluminate inside cementitious materials

After analyzing the figure, one can see that aluminate concentration decreases from 82.5 mol/m^3 to about 62.5 mol/m^3 after reaction. It implies that a depletion of about 20 mol/m^3 have occurred after 400 days of diffusion-reaction process. On the other hand, the maximum sulfate concentration inside the cement stabilized subgrade, without reaction, is 95.5 mol/m^3 which comes down to 70.5 mol/m^3 , meaning about 25 mol/m^3 of sulfate is consumed during the reaction process. The molar ratio of sulfate to aluminate in SA in this simulation yields 1.25, which is a reasonably close with the value reported in the literature as 1.5 (Neville, 2011). Furthermore, as the sulfate proceeds inside cement stabilized subgrades, it reacts with aluminates producing ettringite. In this process, both aluminate and sulfate are consumed. Nevertheless, Figure 2-7 suggests that sulfate concentration increases

from zero to 95.5 mol/m^3 when no reaction is involved. On the other hand, it increases from zero to 70.5 mol/m^3 when it reacts with aluminates. This indicates that in both cases the sulfate concentration increases (with or without reaction). This phenomenon can be explained by the fact that a constant sulfate supply of 82.5 mol/m^3 is provided as a boundary condition at boundary-1. It implies that the model has an unlimited supply of sulfate and the consumption is less than the supply or ingress. This causes the storage of sulfate inside cement stabilized subgrade. It was also observed that at a lower concentration of sulfate in the boundary the sulfate concentration does not always get stored. Because, sometimes it gets drained as well.

Sulfate, Moisture and Heat Migration

After validation of our model sulfate ingress, moisture transport, and heat migration in the simulation with the same settings are further analyzed. The sulfate ingress in cement stabilized subgrade is simulated using a highly nonlinear diffusive equation, and visualization of sulfate propagation front propagation is provided in Figure 2-8.

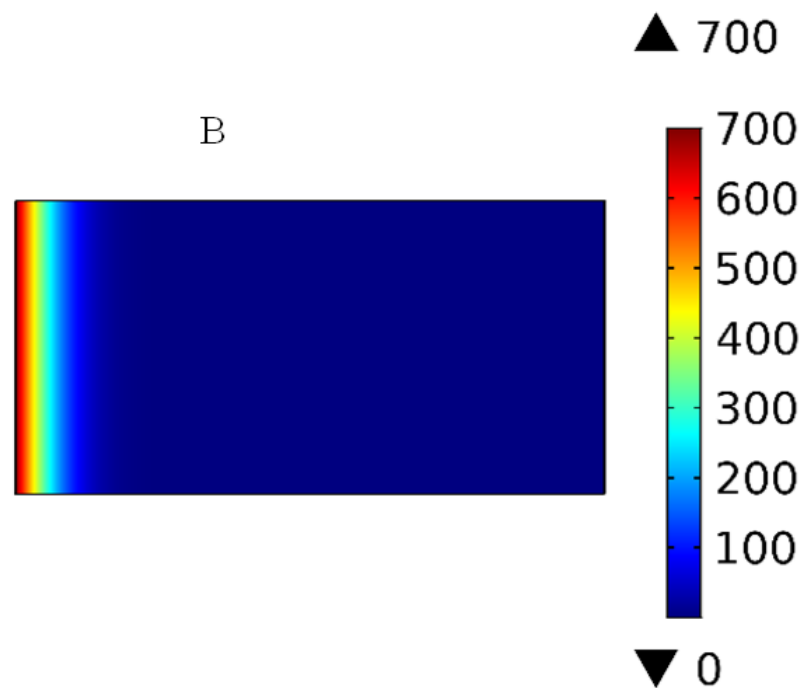
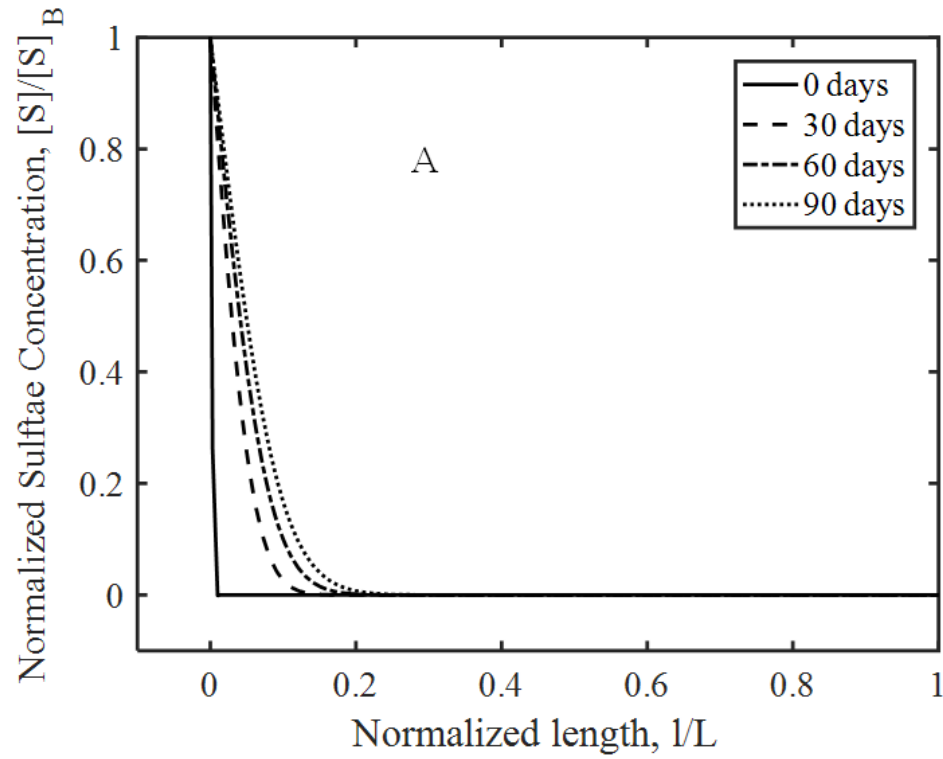


Figure 2-8. (A) Propagation of Sulfate inside cement stabilized subgrade at 0, 30, 60 and 90 days. (B) Distribution of sulfate concentration (mol/m^3) at 90 days.

In Figure 2-8 we can see the propagation of sulfate inside the cement stabilized subgrade sample. Figure 2-8(A) shows the sulfate profile at four different ages; initial condition (0 days), 30, 60, and 90 days. At the beginning (0 days) there is no distribution of sulfate inside the domain. At boundary-1 a Dirichlet boundary condition of 700 mol/m^3 is applied. In this figure, the sulfate concentration and the length are plotted on normal scale. Length is shown in x-axis stretching from 0 to 10 cm and sulfate concentration is shown in y-axis stretching from 0 to 700 mol/m^3 . The coordinates along the plotted lines give sulfate concentration at different position inside the cement-stabilized subgrade sample. For example, from Figure 2-8(A), at the age of 30 days at a length of 0.5 cm the sulfate concentration is 140 mol/m^3 . Figure 2-8(B) visualizes the distribution of sulfate ions in the domain at an age of 90 days. We can see that the maximum sulfate concentration inside the domain is 700 mol/m^3 , located at the left boundary. This distribution of sulfate inside the domain shown in Figure 2-8(B) is represented by the dashed-dotted plot in Figure 2-8(A). The average speed of sulfate propagation was found to be $3.3 \times 10^{-1} \text{ mm/day}$.

Comparing to sulfate diffusion, moisture transport and heat transfer inside cementitious materials is faster. Plots of the degree of saturation and temperature as a function time is provided in Figure 2-9(A) and Figure 2-9(B). From this figure, it can be surmised that the moisture transport inside cementitious materials becomes equilibrium after 5 days of exposure to an environment with a saturation degree of 70%. Heat transport is even faster than fluid transport.

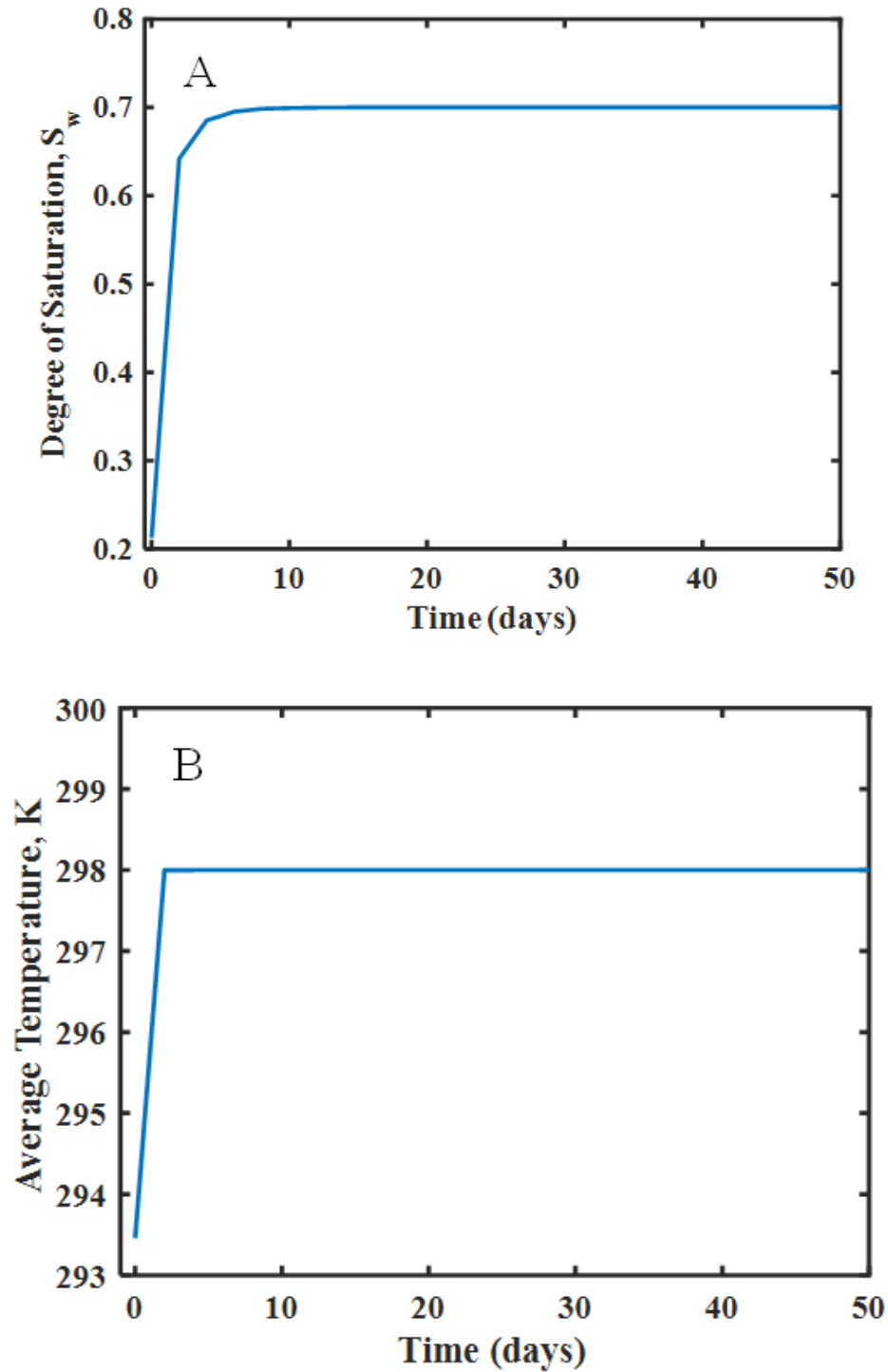


Figure 2-9. (A) Variation of the degree of saturation with time, (B) Variation of temperature with time

Figure 2-9 suggests that an equilibrium heat distribution can be achieved after 2 to 3 days of exposure to the same temperature. For example, if the cement stabilized subgrade

operates at a temperature of $25^{\circ}C$ for 3 continuous days, then the temperature of the entire subgrade will become $25^{\circ}C$. This can be explained by the fact that moisture transport takes place through the pores and depends on the connectivity of the pores, heat conductivity of the fluid. On the other hand, heat transport takes place through both solid and fluid mediums. Thermal conductivity of solid phase is higher than that of fluid phase. This explains why the thermal transport in cementitious materials occurs at a faster rate than moisture transport.

Case Study

For testing the model in an engineering application, we selected a pavement cross-section with four layers to simulate the coupled equations given in Equation 2-25. From top to bottom, the pavement section consists of wearing layer, bounded base, granular subbase, and cement-stabilized subgrade layers. Thermal conductivities of these layers were collected from the literature. The wearing layer and the bounded base had a thermal conductivity of $1.21Wm^{-1}K^{-1}$ (Gui et al., 2007), Sánchez (Díaz-Sánchez & Timm, 2015) assumed a thermal conductivity of $1.16Wm^{-1}K^{-1}$ for the granular base layer. Finally, a thermal conductivity of $0.8Wm^{-1}K^{-1}$ applied for cement stabilized subgrade layer.

Please note that only boundary condition for thermal transport was applied on the top boundary, so, thermal transport took place through different layers of pavement. As a result, different thermal conductivities were used for different layers. Other equations, such as moisture and sulfate migrations were applied only on the bottom layer, since, this layer is of our interest to observe the deterioration effect of sulfate attack. Hence, the material properties of other layers for simulating these equations was not required. A schematic of the model with dimension is provided in Figure 2-10.

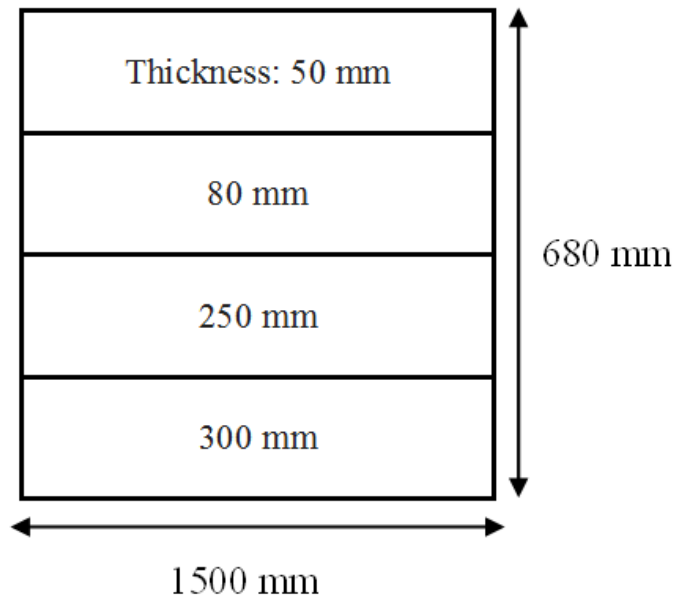


Figure 2-10. Schematic diagram of the model adopted for a case study

In this model, a temperature difference was applied on top and bottom of the model. At the top layer, we applied a sinusoidal variation of temperature using Equation 2-32.

$$T_b = 20 + 10 \times \sin(2\pi t) \quad (2-32)$$

Here, t is time in days, and the output is in degree celsius. This sinusoidal variation of temperature is adopted to imitate the temperature variation during the day. According to this equation, temperature varies from 10°C to 30°C . The bottom boundary of the domain is in contact with soil so that the temperature at the bottom is considered constant. Thus, a dirichlet boundary condition of 10°C is applied. For migration of moisture, the entire domain is considered for simulation, whereas only the bottom layer is considered for SA. This is due to the fact that the top three layers are not cement stabilized and we are only interested with cement stabilized layer under SA. Sulfate concentration as boundary condition is applied from the bottom. As it is assumed that the cement stabilized layer is in

contact with soil. Therefore, sulfate solution can reach cement stabilized subgrade only from the bottom. Moisture also migrates inside through the bottom layer.

Variation of the degree of saturation, Figure 2-11(A), and temperature, Figure 2-11(B), in the pavement section are shown in the following figure indicating the change after one month from the beginning of SA.

Clearly, there is a gradient of temperature and saturation degree inside the domain as seen in Figure 2-11.

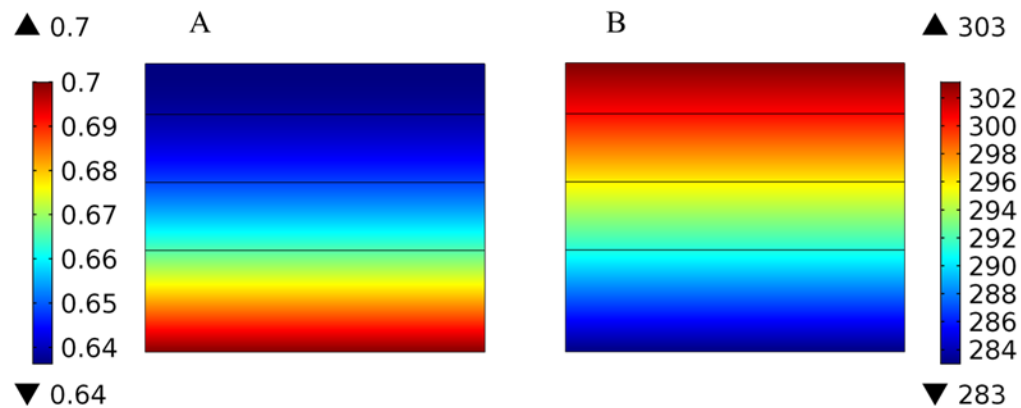


Figure 2-11. Simulation results at one month: (A) Variation of Degree of saturation, (B) Variation of Temperature (K)

From Figure 2-11(A) we can see that the degree of saturation varies from 0.64 to 0.7. This signifies the fact that after one month the degree of saturation of the model increased from 0.2 (the initial condition) to 0.64. On the other hand, the temperature of the domain, shown in Figure 2-11(B), varies from **283K (10°C)** to **303K (30°C)**. An equilibrium state of degree of saturation is achieved after 100 days from the beginning of simulation, whereas temperature takes only 5 days to attain equilibrium state. Thus, the layered pavement system intends to achieve equilibrium temperature very quickly

compared to moisture migration. Figure 2-12 shows the profile of sulfate concentration, stress, and strain after 4 months.

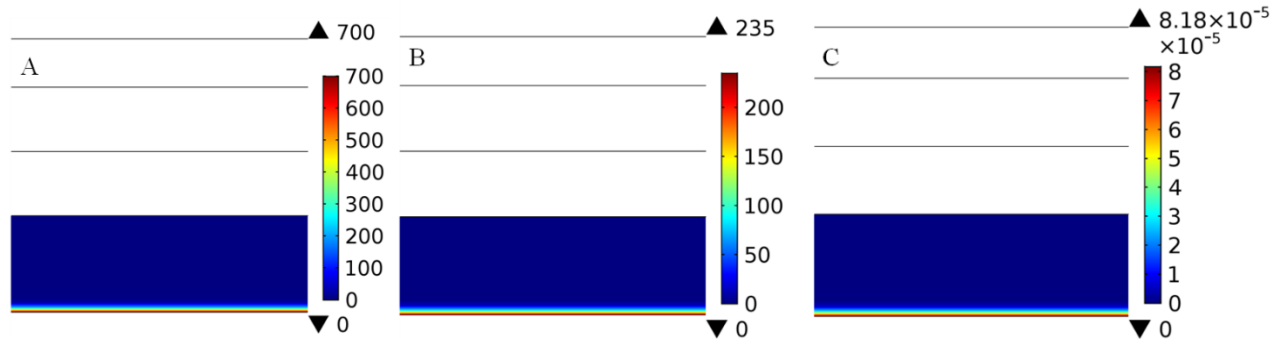


Figure 2-12. Simulation results at four months: (A) Sulfate migration inside concrete, (B) Stress induced by diffused sulfate (psi) (C) Stress induced by diffused sulfate (mm/mm)

Figure 2-12(A) shows the sulfate migration inside concrete. Initially, the block was assumed free from sulfates. This explains the zero value everywhere inside the subgrade, except the region where sulfate gets diffused. The average sulfate concentration inside subgrade after 4 months is 81.5 mol/m^3 . Figure 2-12(B) shows the stress induced by the expansion, which induces a tensile stress in material. The maximum stress inside concrete is 235 psi . No compressive stress was present, since the stress is induced by SA-induced expansion without involvement of any mechanical loads. Finally, Figure 2-12(C) shows the strain due to SA, which illustrates that strain in cementitious material reach up to $8.18 \times 10^{-5} \text{ mm/mm}$ due to SA after 4 months.

After analyzing the expansive stress and eigenstrains induced by SA, we concentrate on the failure predicting model. Figure 2-13 shows the DP yield criterion on the model. This is a stress-dependent model for determining whether the material has failed or undergone plastic yielding. The red zone in the figure indicates the mechanically

damaged locations, while the blue zone indicates the safe zone. From the close view, we can see that DP function determined damaged location 0.4 cm (4 mm) inside the bottom boundary.

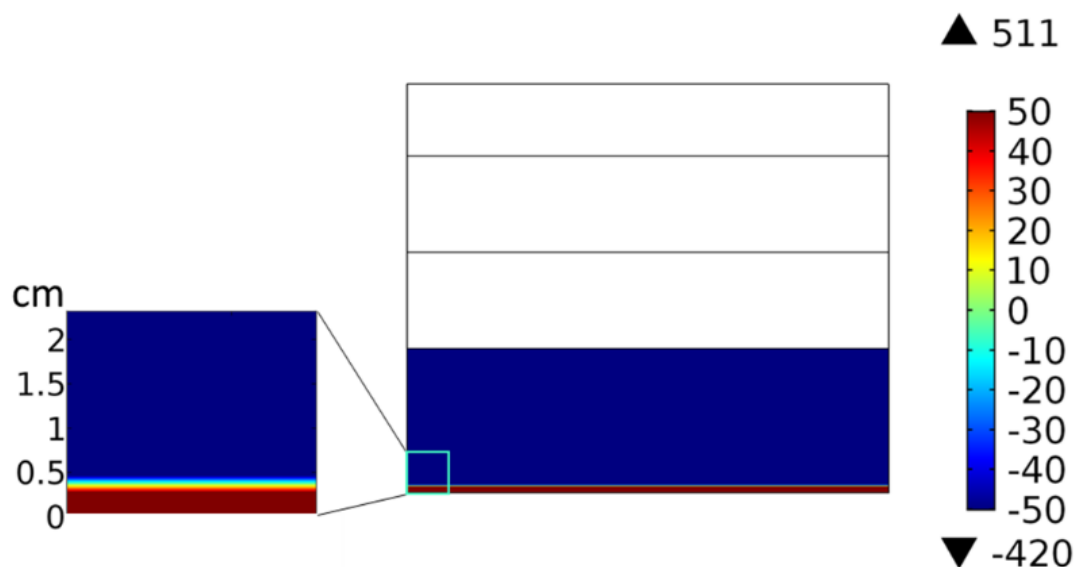


Figure 2-13. Failure indicated by DP yield criterion

The sulfate penetrates 0.5 cm (5 mm) inside of the subgrade layer from the boundary. The average penetration rate from depth of penetration of sulfate is estimated to be $4.2 \times 10^{-2}\text{ mm/day}$. This value is lower than the previously calculated average speed of $3.3 \times 10^{-1}\text{ mm/day}$. This is due to the fact that in the validation model the heat and moisture were migrating through the same boundary, which in turn accelerated the propagation rate of moisture and dissolved sulfate. Now, from sulfate profile we obtained that the concentration at a height of 4 mm is approximately 600 mol/m^3 . This signifies the fact that the specific zone will be damaged when the sulfate concentration inside cementitious materials exceeds 600 mol/m^3 .

Conclusion

Although the process of SA in cementitious materials is well known and the researchers are aware of the adverse effect of it, a comprehensive mathematical model to predict long-term damage effects was unavailable. Hence, an extensive model is needed to simulate sulfate propagation and predict mechanical stress and damage. In this work, we proposed a chemo-mechanical model of SA in cement stabilized pavements. The CM model for cement stabilized subgrade of SA was established with considerations of heat and degree of saturation. The contribution of this paper is that the internal expansion-induced mechanical and damage effects are calculated by including the unsaturated condition effects and coupled with non-isothermal heat transfer. It is an improvement from existing sulfate attack damaging models, which only considers diffusion in a fully saturated media or an isothermal environment.

To verify the CM model, we simulated an experiment conducted by Condor (Condor et al., 2011). The results from the simulation matched very well with the experimental results. For further validation of the model, the molar ratio of the reactants participating in the reaction was determined. The molar ratio found from the simulation is 1.25, whereas the actual value is 1.5. This shows a good match between the reaction and simulation output. In the field, an equilibrium state of moisture distribution can be achieved after a few months from the beginning of moisture transport. On the other hand, temperature takes only several days to reach equilibrium. Thus, the layered pavement system intends to achieve equilibrium temperature quite fast compared to moisture migration.

Furthermore, we combined the models proposed by Santhanam (Santhanam et al., 2002) and Ming (Ming et al., 2016) to predict the mechanical behavior of cementitious material undergoing SA. This combined model was used to estimate the eigenstrain and corresponding mechanical damage along with the stress of cementitious materials under SA. We found that if the sulfate concentration reaches 600 mol/m^3 , the material will fail. We also used DP yield criterion to determine the mechanically damaged zone of cementitious material under SA. It was found that after a period of four months the sulfate penetration depth was about 5 mm and the penetration depth depends on temperature of the domain.

In general, the simulation results coincide with our expectation that part of the sulfate ingressed into subgrade has reacted with the available aluminates and formed ettringite. Thus, the accumulation of sulfate concentration within the subgrade is retarded by the chemical reaction. With age the integrity of the pavement structure gets reduced, the chemical reaction induced internal expansion forces that accelerate the mechanical damage process.

REFERENCES

- Bary, B. (2008). Simplified coupled chemo-mechanical modeling of cement pastes behavior subjected to combined leaching and external sulfate attack. *International Journal for Numerical and Analytical Methods in Geomechanics*, 1891-1816.
- Basista, M., & Weglewski, W. (2008). Micromechanical modeling of sulfate corrosion in concrete: influence of ettringite forming reaction. *Theory of applied mechanics*, 29-52.
- Basista, M., & Weglewski, W. (2009). Chemically assisted damage of concrete: a model of expansion under external sulfate attack. *International Journal of Damage mechanics*, 155-175.
- Cefis, N., & Comi, C. (2017). Chemo-Mechanical modeling of the external sulfate attack in concrete. *Cement and Concrete Research*, 57-70.
- Clifton, J., & Pommersheim, J. (1994). *Sulfate Attack of Cementitious Materials: Volumetric*. NISTIR 5390.
- Condor, J., Asghari, K., & Unatrakarn, D. (2011). Experimental Results of Diffusion Coefficient of Sulfate Ions in Cement Type 10 and Class G. *Energy Procedia* 4, 5267-5274.
- Coussy, O. (2004). *Poromechanics*. John Wiley & Sons.
- Croft, J. B. (1967). The influence of soil mineralogical composition on cement stabilization. *Geotechnique*, 119-135.
- Díaz-Sánchez, M. A., & Timm, D. H. (2015). Influence of Sustainable Technologies on In-Place Thermal Properties of. *Airfield and Highway Pavements* , 536-547.
- Drucker, D. C., & Prager, W. (1952). Soil mechanics and plastic analysis for limit design. *Quarterly of Applied Mathematics*, 157-165.

- Fu, Y., Xie, P., Gu, P., & Beaudoin, J. J. (1994). Significance of preexisting cracks on nucleation of secondary ettringite in steam-cured cement paste. *Cement and Concrete Research*, 1015-1024.
- Gui, J. (., Phelan, P. E., Kaloush, K. E., & Golden, J. S. (2007). Impact of Pavement Thermophysical Properties. *Journal of Materials in Civil Engineering*, 683-690.
- Hoglund, L. (1992). Some notes on ettringite formation in cementitious material- Influence of hydration and thermodynamic constraints for durability. *Cement and Concrete Research*, 271-228.
- Jacobsen, S., & Sellevold, E. J. (1996). Self-healing of high strength concrete after deterioration by freeze/thaw. *Cement and Concrete Research*, 55-62.
- José, J., & Cela, L. (1998). Analysis of reinforced concrete structures subjected to dynamic loads with a viscoplastic Drucker–Prager model. *Applied Mathematical Modelling*, 495-515.
- Lawrence, C. (1990). Sulfate Attack on Concrete. *Magazine of Concrete Research*, 249-264.
- Laidler, K. J. (1984). The development of the Arrhenius equation. *Journal of Chemical Education*, 494.
- Lide, D. (2003). *CRC handbook of chemistry and physics*, 84th Ed. Boca Raton, Fl: CRC Press.
- Little, D. N., & Nair, S. (2009). Recommended practice for stabilization of sulfate-rich subgrade soils. NCHRP.
- Ming, F., Deng, Y.-s., & Li, D.-q. (2016). Mechanical and Durability Evaluation of Concrete with Sulfate Solution Corrosion. *Advances in Material Sciences and Engineering*, Hindawi.
- Neville, A. (2011). *Properties of Concrete*. Essex, England: Pearson Education Limited.
- Nield, D. A., & Bejan, A. (2017). *Convection in Porous Media*. NY: Springer.
- Ping, X., & Beaudoin, J. (1992). Mechanism of sulfate expansion I. Thermodynamic principle of crystallization pressure. *Cement and Concrete Research*, 631-640.

- Rollings, R. S., Burkes, J. P., & Rollings, M. P. (1999). Sulfate Attack on Cement-Stabilized Sand. *Journal of Geotechnical and Geoenvironmental Engineering*, 364-372.
- Samson, E., J. Marchand, K. S., & Beaudoin, J. (2005). Modeling ion and fluid transport in unsaturated cement systems in isothermal conditions. *Cement and Concrete Research*, 141-153.
- Santhanam, M., Cohen, M. D., & Olek, J. (2002). Mechanism of sulfate attack: A fresh look: Part 1: Summary of experimental result. *Cement and Concrete Research*, 915-921.
- Sarkar, S., Mahadevan, S., Meeussen, J., Sloot, H. v., & Kosson, D. (2010). Numerical simulation of cementitious materials degradation under external sulfate attack. *Cement and Concrete Composites*, 241-252.
- Skalny, J., Marchand, J., & Odler, I. (2001). *Sulfate Attack on Concrete*. London: Spon Press.
- Tixier, R., & Mobasher, B. (2003). Modeling of Damage in Cement-Based Materials Subjected to External Sulfate Attack. II: Comparison with Experiments. *Journal of Materials in Civil Engineering*, Vol. 15, No. 4,, 314-322.
- Yuan, Q., Shi, C., Schutter, G. D., & Audenaert, K. (2009). Effect of temperature on transport of chloride ions in concrete. *Concrete Repair, Rehabilitation and Retrofitting II*, 345-351.

CHAPTER THREE: COUPLED THERMO-CHEMO-MECHANICAL MODELLING
OF CONCRETE DURABILITY SUBJECTED TO COMBINED SULFATE ATTACK
AND FREEZE-THAW CONDITIONS

Abstract

Concrete structures experience damage due to Sulfate Attack (SA) and Freeze-Thaw (F-T) in cold regions containing ample amount of sulfate species. The combined effect of SA and F-T is a multiscale multiphysics damaging process for cementitious materials involving complicated chemical reactions and phase change inside concrete pores. This paper presents a theoretical model of this phenomenon using the classical theory of phase change and a diffusion-reaction process. A comparison of the numerical results with existing experimental data for concrete mortars illustrates the validity of the proposed model. This coupled mathematical model can be applied in assessing the effect of the pore-size distribution (PSD), the hysteresis of solidification and melting of water in concrete pores and the change of porosity due to SA and F-T, especially the factors that are difficult to evaluate by current experimental methods.

Author keywords: Concrete; Freeze-Thaw; Sulfate Attack; Deterioration; Damage Evaluation.

Introduction

The durability of concrete structures has been a concerning topic to civil engineers for a long time. It is a well-known fact that cementitious materials subjected to environmental ingresses experience loss in mechanical stability and durability due to several factors. For example, moisture and heat transport can cause degradation that weakens the microstructure of cementitious materials. F-T phenomenon nucleates microcracks by inducing expansive stress (Jacobsen, S. and Sellevold, E.J. 1996). SA carbonation or the chloride intrusion acts on damaging concrete in a similar process by generating expansive stress. There are numerous examples of SA caused damages of concrete around the world. For instance, Elbe River bridge piers in Magdeburg, East Germany suffered excessive expansion due to sulfate content in the water (2040 mg/l) and resulted in a rise of the piers by 8cm in just 4 years. Similarly, increase in porosity was observed in Fort Peck dam located in Montana, US. The ambient temperature in the stated geographic locations can drop below the freezing temperature of the water during the winter seasons. There also exists a large volume of sulfate-abundant soil and more than 1000 salt lakes scattered around Northwest China (Jiang, Niu, Yuan, & Fei, 2015). SA on cement-based materials coupled with F-T damage is a severe problem affecting the durability and service life of concrete structures. Structures in those regions mentioned above are damaged principally due to the combined effect of SA and F-T damage. For instance, concrete porosity gets increased due to SA leaving more space for water. Afterward, the accumulated water gets frozen inside the additional porosity, more stress-strain gets generated. This exacerbating phenomenon plays the critical role to accelerate the civil infrastructure degradation leading to premature failure and serious aging

problems. A concept map of the interaction between temperature SA and F-T is shown in Figure 3-1.

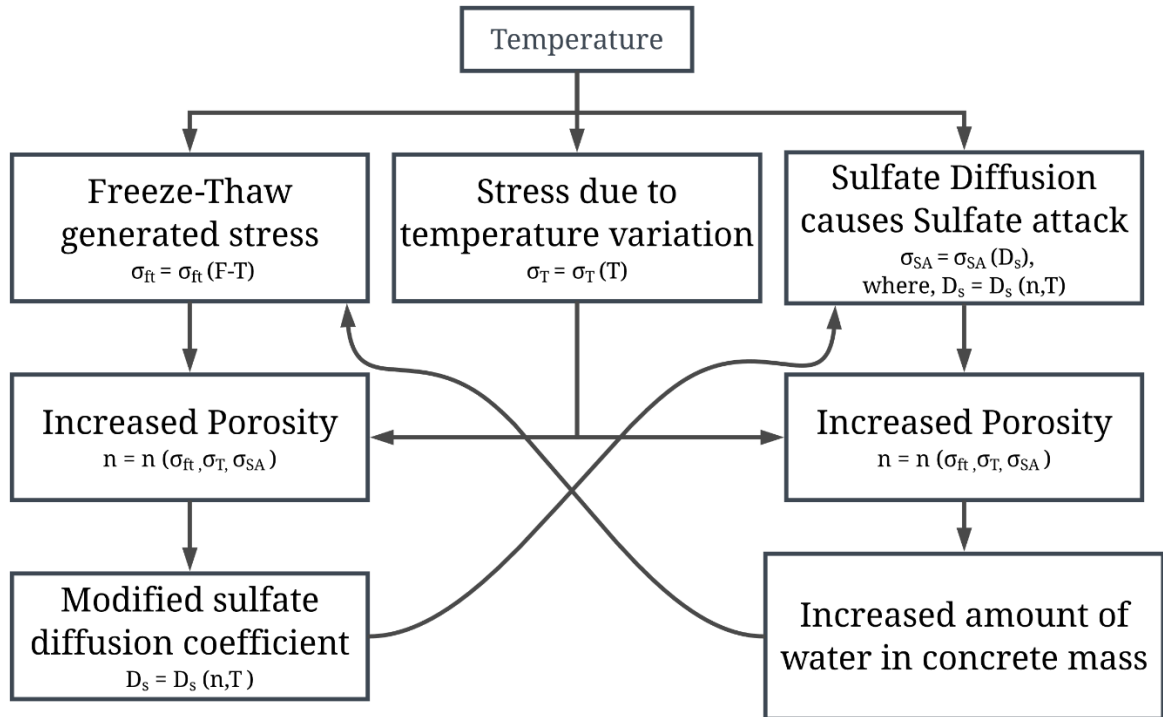


Figure 3-1: Concept map of interaction between SA and F-T

In addition to the above mentioned detrimental effects of SA and F-T, temperature variation also has a detrimental effect on concrete durability. Although it is not considered in the developed model, rapid variation in temperature may cause thermal shrinkage-expansion as well as thermal fatigue in concrete structures. These effects eventually accelerate the deterioration of concrete structures. Therefore, it is of utmost importance to understand the damage process of the concretes due to combined SA and F-T to predict their remaining service life and designing concrete suitable for these environmentally aggressive locations.

Despite many improvements in materials and methods of construction, still, a lot of concrete structures fail prematurely. This leads to costly and time-consuming repairs. In

recent years, researchers have achieved great success in the study of concrete durability. A large number of tests have been conducted in the study of single factor damage on concrete (Long, Xie, & Tang, 2007). For example, Lu et al. (Lu, Garboczi, Bentz, & Davis, 2012) studied chloride transport in cracked concrete, Basista et al. (Basista & Weglewski, 2009) and Cefis et al. (Cefis & Comi, 2017) studied the sulfate induced damage in concrete. Modeling and experimental investigation of carbonation of concrete are conducted by Papadakis et al. (Papadakis, Vayenas, & Fardis, 1991) and so on. These works are a short collection from a vast database of literature on the investigation of degradation processes due to environmental factors. Furthermore, these works focused on damages caused by single degradation mode (i.e. alkali silica reaction), which could be one of the major reasons of practical engineering failures. Nevertheless, in the case of field situations, the coexistence of more than just one aggressive agent is usual. The interactions of these individual degradation modes may further influence the durability of concrete (Niu, Jiang, & Fei, 2013). For example, ettringite produced due to SA, reduces the porosity decreasing the ability of concrete to compensate for expansion due to freezing, which is a positive effect. On the other hand, localized damages caused by F-T (e.g. microcracks on pore walls) increases concrete permeability, amplifying the diffusivity of sulfate (Piasta, Marczevska, & Jaworska, 2015), which is a negative effect. These complex interactions increase the nonlinearity of the mechanisms governing the deterioration of concrete structures. However, the governing mechanisms of this complex interaction behavior are not known yet. Therefore, in order to predict the degree of damage to the concrete structures under such environmental conditions, more fundamental research should be focused on studying their coupled interaction caused by multiple degradation modes on

damage process. Knowing the level of damage will assist engineers to offer better preservation plan and maintain the mechanical performance of the structure, thus increasing the service life of the structures. Most importantly, locations having significant damage can be monitored and precautions can be taken in order to prevent catastrophic failure.

According to literature, concrete deterioration due to sulfate attack alone is the second significant durability related issue, the corrosion of reinforcement bars being in first place (Al-Dulaijan et al., 2003). Once frost-related decay starts interacting with the SA process, concrete deterioration gets exacerbated. Such types of detrimental effect is prevalent principally in geographical regions with the frequent oscillation of temperature around the freezing temperature of water and has free sulfate in their ambiance. The concrete structures suffer from F-T damage when the ambient temperature falls below the freezing point of water. Concrete in these cold regions experiences both damages from both SA and F-T cycles. Therefore, concrete deterioration due to the combined effect of SA and F-T damage is a serious issue. It has a serious adverse impact on the durability of concrete. This eventually impacts the service life of concrete structures (Skalny, Marchand, & Odler, 2003). Unfortunately, current research efforts offer a limited amount of literature on the coupled deterioration of concrete undergoing F-T and SA damage.

The damage of concrete, when exposed to sulfate solutions, has been a concern to civil engineers for many decades. The sulfate ions present in groundwaters migrate through the capillary pores of concrete driven by the gradient of concentration. Complex chemical reactions get triggered upon contact between active components of the hardened cement paste and the migrated sulfate (Neville, A.M, 1981). The expansive products of such

reactions may cause microcracking and overall expansion of a structural element (Skalny et al., 2003). The ettringite formed during this process is called the secondary ettringite to distinguish it from the primary ettringite formed during the hydration of cement. SA may be external or internal depending on the source of the sulfate ions. As the name suggests, if the damage is caused by migratory sulfate, then it is called External Sulfate Attack (ESA), and if sulfate is present in the domestic material, then it is called Internal Sulfate Attack (ISA). The source can be the cement, supplementary materials such as fly ash or slag, the aggregate, the chemical admixtures, or even the water used to produce the mix (Neville, A.M, 1981). It is noteworthy that the expansive products generated due to ISA and ESA are source independent. Nevertheless, the damage due to ISA is comparatively less due to the fact that the availability of sulfate is limited in case of ISA, while the ESA depends on the external source of sulfate.

Damage due to sulfate attack is caused by the generation and precipitation of expansive products engendered by the reaction between C3A and sulfate ions. This generates tensile stress on the pore walls, which is responsible for the generation of microcracks due to SA. Furthermore, when the ambient temperature drops below the freezing point of water, it undergoes a phase transition from liquid to solid (ice). Ice occupies 9% more volume than that of water. If the concrete sample under study is fully saturated, there will be no space to accommodate this volume expansion in pores. Additional volume reduction of pores occurs due to precipitation of ettringite, which exacerbates the internal expansion stress in those zones of concrete. As water freezes, frozen water will start exerting expansive/tensile stress on the pore stress to adapt to the extra volume due to phase change. Distresses due to critically saturated concrete from F-T

will commence with the initial F-T cycle and will continue throughout successive periods in the winter seasons, causing repeated loss of concrete mechanical properties.

As previously stated, for the past several decades, researchers have been studying the degradation of concrete due to either sulfate attack or F-T cycles. The degradation behavior of concrete under coupled F-T and SA conditions has yet to be understood. Several experimental studies have been conducted to investigate the combined detrimental effect of F-T cycles coupled with sulfate attack. Miao et al. (Miao, Mu, Tian, & Sun, 2002) examined the response of concrete subjected to F-T cycles in sodium sulfate solution. It was confirmed by their research that the combined interaction of sulfate attack and F-T cycles accelerates the deterioration mechanism of concrete structures. Concrete samples containing steel-fiber-reinforced concrete (SFRC) was casted in order to evaluate the improvements in durability due to the application of SFRC. Plain concrete and SFRC, with different water-cement ratios of up to 0.44, undergone F-T cycles immersed in 5% sodium sulfate solution and pure water. Results showed that the properties of SFRC are superior to those of plain concrete. Relative dynamic modulus of elasticity (RDME) of SFRC gets reduced comparatively slower than that of plain concrete with increasing F-T cycles. In other words, the application of SFRC improves the F-T resistance capability, which is supported by the findings from Sun et al. (Sun, Zhang, Yan, & Mu, 1999).

A similar experimental study was conducted by Jiang et al. (Jiang, Niu, Yuan, & Fei, 2015) using similar experimental setup. In addition to the procedure adopted by Miao et al. (Miao et al., 2002), they added a magnesium sulfate solution to evaluate the effect of different sulfate solutions on concrete deterioration along with F-T cycles. They concluded that sulfate attack, although detrimental to concrete durability, has positive effect on F-T

resistance of concrete by lowering the freezing point of the solution. This result is corroborated through research findings by Wang et al. (Wang, Zhou, Meng, & Chen, 2017). On the other hand, the diffusion process gets halted once the solution gets frozen. This, ultimately, stops the detrimental reaction caused by SA. However, as the F-T cycle continues, damage gets accumulated, and RDME loss becomes prominent. RDME loss occurs at a faster rate when the sample is immersed in a magnesium sulfate solution concluded from the investigation by Jiang et al. (Jiang et al., 2015). This is due to the fact that magnesium sulfate is usually more aggressive compared to sodium sulfate because magnesium sulfate participates in both expansions of the cement paste and decalcification of the calcium silicate hydrate (CSH) (Basista & Weglewski, 2009). However, a similar trend was observed in RDME loss in both water and sodium sulfate solutions.

Wang et al. systematically investigated the response of concrete containing fly ash and silica fume subjected to coupled F-T and SA. They observed that the replacement level of 25% fly ash and 5–8% silica fume by weight improves the resistance of concrete against the coupled F-T and SA. F-T and sulfate attacks. Yang et al. (Yang, Shen, Rao, Li, & Wang, 2015) employed advanced test methods to investigate the effects of sulfate attack and F-T cycles on concrete microstructure. Their experimental results indicated that F-T damage is the most contributing factor in coupled SA and F-T alternation tests. They also produced concrete samples with 20% fly ash and summarized that fly ash acted as micro-aggregates and improved the pore size distribution as well as durability of concrete in an adverse environment with F-T cycles and SA.

Li et al. (Y. Li, Wang, Li, Zhao, & Qin, 2018) studied the effect of the coupled F-T cycles and SA on the durability of concrete containing low-volume fly ash (LVFA) and

high-volume fly ash (HVFA). Their concrete samples had a water-cement (W/C) ratio of 0.50 with fly ash and recycled aggregates different percentages by weight as a replacement for coarse natural aggregates (CNA). These samples were exposed to water, 5% sodium sulfate solution and 5% magnesium sulfate solution along with F–T cycles. The loss of compressive strength, RDME, and concrete microstructure was evaluated at specific F–T cycles in sulfate solutions. They found that the resistance of the concrete mixtures to the combined F–T cycles and SA got improved with the increase in CRCA content. Compared to the concrete without FA, the LVFA-based concrete showed better improvement in the resistance to the combined action of F–T cycles and SA.

Note that the damage caused by SA is a prolonged process. In order for the detection of actual damage the concrete samples need to be submerged in a concentrated sulfate solution for a long time. Piasta et al. (Piasta et al., 2015) experimented SA and F-T attacks on air entrained and non-air-entrained mortar samples under two conditions. After prior F-T the mortar bars were subjected to SA of the 5% ($355\text{mol}/\text{m}^3$) Na_2SO_4 solution. Another part of the mortar bars were submerged in the same sulfate solution for 110 days and afterwards subjected to F-T. They concluded that air entrainment is actually detrimental for the SA durability of concrete, since the distribution of pores for air entrainment increased the connectivity of pores, which in turn increased the permeability of concrete. In contrast, non air-entrained samples performed poorly in case of F-T damages.

The above brief survey enlightens that the field of coupled damage process due to the combined effect of F-T and sulfate attack has been under experimental study so far. These existing experimental studies found that the combined impact of F-T and sulfate

attack is a nonlinear behavior. The mechanical damage caused by this nonlinear effect is a complex phenomenon and not well understood yet. Moreover, damage caused by SA is a slow process that occurs over a long period of incubation. Most of the discussed experimental studies tested F-T and SA damage within the time limit of freeze-thaw cycles. Usually, one F-T cycle occurred within four to six hours that included both Freezing and thawing part of F-T. Therefore, actual damage caused in these tests was mainly from F-T. This research focuses on investigating the durability of concretes exposed to these combined modes of deterioration through a fundamental understanding of this process. In this work, we study the coupled interaction between SA and F-T using a comprehensive Thermo-Chemo-Mechanical (TCM) framework. The developed mathematical model will be useful to observe actual damage caused by both F-T and SA. The freezing model is based on a model published by Bazant et al. (Bazant, Chern, Rosenberg, & Gaidis, 1988). Sulfate diffusion model is based on author's previously published work (Islam, Golrokh, & Lu, 2018). The following sections are devoted to explaining different aspects of the model, such as, modeling sulfate diffusion, the phase transition of water in concrete pores, and the pressure generated due to the expansion of ettringite and ice formation.

Coupled F-T and SA Equation Set Derivation

Freezing Theory of Porous Structures

In a freezing environment, ice crystals grow by transforming more and more water into ice. Ice has a lower chemical potential than that of water, and according to thermodynamics all the materials have an inherent tendency to reduce the overall potential to dwell in a lower energy state. Consequently, when the temperature gets decreased a driving force for water to transform into ice gets generated. Now if the chemical potential

of ice and water is defined by μ_i and μ_w respectively, then the change in chemical potentials can be found using equations 3-1 and 3-2.

$$d\mu_i = -S_i dT + v_i dp_i \quad (3-1)$$

$$d\mu_w = -S_w dT + v_w dp_w \quad (3-2)$$

Here, μ is the chemical potential of each species, S is molar entropy given by Gibbs-Duhem equation (Scherer, 1992), v is molar volume, and p is pressure in individual species. Subscripts w and i denotes water and ice fraction in pores.

Chemical potentials are equal ($d\mu_i = d\mu_w$) along the ice water interface. If we consider that the liquid fraction does not experience any change in pressure ($dp_w = 0$) then we find,

$$dp_i = \frac{S_i - S_w}{v_i} dT \quad (3-3)$$

At triple point (T_m) the water, ice and vapor stay in equilibrium and pressure on the crystal is p_m . This pressure changes to p_A at a temperature (T) different from T_m . Therefore, the limit of integration for pressure is p_m to p_A and for temperature is T_m to T . Integrating equation 3-3 within the stated limit we get,

$$\int_{p_m}^{p_A} dp_i = \int_{T_m}^T \frac{S_i - S_w}{v_i} dT$$

$$P_A - P_m = \frac{S_i - S_w}{v_i} (T - T_m) = \Delta S_{iw} \Delta T \quad (3-4)$$

here, $\Delta S_{iw} = \frac{S_i - S_w}{v_i}$, with v_i being the molar volume of ice, is the entropy of fusion per unit volume of crystal and $\Delta T = T_m - T$ is the change in temperature. This equation correlates energy difference between ice crystal and water. According to Scherer (Scherer, 1999) the value of entropy per unit volume of the crystal is taken as $\Delta S_{iw} = 1.2 \frac{J}{cm^3 K}$.

A relation between pressure in ice (p_i) and pressure in water (p_w) can be found using Laplace's formula given in equation 3-5 (Duan, Chen, & Jin, 2013)

$$p_i = p_w + \gamma\kappa_{iw} \quad (3-5)$$

here, γ is the energy of ice water interface and the adopted value is $39 \times 10^{-3} \text{ N/m}$, $\kappa_{iw} = \frac{1}{r_1} + \frac{1}{r_2}$ is the curvature of ice/water interface, with r_1 and r_2 being the principle radii of curvature. For a spherical pore r_1 and r_2 is equal ($r_1 = r_2 = r$) and the curvature equation reduces to $\kappa_{iw} = \frac{2}{r}$, here r is the radius of the spherical pore. Hence, we can rewrite equation 3-5 as follows (K. Li, 2016 (Ch 3)),

$$p_i = p_w + \frac{2\gamma}{r} \quad (3-6)$$

Fagerlund (Fagerlund, 1973) showed that there is a thin layer of water that is adsorbed on the pore wall and does not get frozen. Thickness (r_a) of this layer is given in equation 3-7.

$$r_a = -d * \left(\frac{A}{\ln\left(\frac{p}{p_0}\right)} \right)^B \quad (3-7)$$

Here, A and B are constants taken as 1.63 and 1/3 respectively, d is the diameter of the water molecule ($\approx 3.5 \text{ \AA}$) and $\frac{p}{p_0}$ is the relative vapor pressure. $\ln\left(\frac{p}{p_0}\right)$ is related to freezing point depression (ΔT) and is given by equation 3-8 (Puri, Sharma, & Lakhdnpal, 1954).

$$\ln\left(\frac{p}{p_0}\right) = 0.9686 \times 10^{-2} \Delta T - 0.56 \times 10^{-6} (\Delta T)^2 + 0.72 \times 10^{-8} (\Delta T)^3 \quad (3-8)$$

Here, $\Delta T = T_{f0} - T_f$ is the freezing point depression, where, T_{f0} is the freezing temperature at reference vapor pressure, p_0 and T_f is the freezing temperature at pressure,

p. Equation 3-8 exploits a freezing point depression term, which is computed using equation 3-9 (Jallut, Lenoir, Bardot, & Eyraud, 1992).

$$\Delta T = \frac{2}{r} \times \frac{\gamma}{\Delta S_{iw}} \quad (3-9)$$

Note that, γ and ΔS_{iw} in equation 3-9 are constants. Therefore, the depleted freezing point varies reciprocally with the radii of the pores. Using the values of γ and ΔS_{iw} for a 100nm pore the value of ΔT is calculated to be 0.65K. Meaning that, a pore with a radius of 100nm will freeze at 0.65K (or 0.65°C) below the actual freezing point. However, this equation considers that the pore water is saturated with pure water. Freezing point depression due to the presence of sulfate needs to be considered in equation 3-9. Ebbing et al. (Ebbing & Gammon, 2009) showed that the freezing-point is correlated to the concentration of the solution. Here, it is noteworthy that the depression of freezing point is a colligative property. Colligative properties, as defined by Ebbing (Ebbing & Gammon, 2009) are properties of solutions that depend on the concentration of solution but not on the chemical properties of the solute. In other words, chemical properties of solution do not have any influence on the lowering of freezing point of the solvent. Hence, freezing point depression of a solution is proportional to the molal concentration (c_m) and is given by,

$$\Delta T_{solution} = k_b c_m \quad (3-10)$$

here, k_b is a proportionality constant and for water and a widely accepted value is 1.86K/m, meaning a 0.5 m solution freezes at 0.93°C below the freezing point of pure water, and c_m is the concentration of the solution expressed in molality. Molality of a solution is defined as the number of moles dissolved in 1kg of solvent. Combining

equations 3-9 and 3-10 yields the freezing point depression of sulfate solution inside concrete pores.

$$\Delta T = \frac{2}{r} \times \frac{\gamma}{\Delta S_{iw}} + k_b c_m \quad (3-11)$$

Using equation 3-11 the smallest size of the pore that will freeze at a given freezing temperature can be calculated. An alternate procedure was shown by Setzer (Setzer, 2000).

Where the radius, r , of smallest pore that freezes at a temperature, θ in °C, is given by,

$$r = \frac{64}{|\theta|} \text{ (nm)} \quad (3-12)$$

From equation 3-9, it was evaluated that water in a 100 nm pore freezes at -0.65°C . Using this freezing temperature equation 3-12 yields 98.5nm which is pretty close to 100nm that was taken as an input parameter to equation 3-9. This equation is also valid for a pure solution only and to consider the effect of solution a shift in θ should be applied. Upon applying the shift in freezing point temperature θ equation 3-12 reads,

$$r = \frac{64}{|\theta + k_b c_m|} \text{ (nm)} \quad (3-13)$$

Using the same freezing temperature of -0.65°C and considering a solution molal concentration of 0.5m equation 3-13 yields 220.5 nm. It denotes that further reduction in temperature is required for freezing the pores with a radius of 100nm when sulfate is present in the water. Note that freezing point depression due to a solution on porous structures is included by the authors to introduce the coupling between depletion of freezing point and solution concentration.

Equation 3-13 together with equation 3-7 provides the smallest pore radius that gets frozen at a given temperature and is given by,

$$r_f = \frac{64}{|\theta + k_b c_m|} - d * \left(\frac{A}{\ln\left(\frac{p}{p_o}\right)} \right)^B \quad (\text{nm}) \quad (3-14)$$

here, r_f is the smallest radius of the pore that gets frozen. Note that, $\ln\left(\frac{p}{p_o}\right)$ makes use of freezing point depressing expressed by equation 3-11.

Phase Transition in Pores

In the previous section the freezing mechanism inside a porous structure is discussed. This section is devoted for the discussion of energy balance due to a phase transition. First of all, the heat transfer equation for a phase transitioning liquid is proposed by Bazant et al. (Bazant et al., 1988) and shown in equation 3-15.

$$\rho C \frac{\partial T}{\partial t} = \nabla \cdot (\lambda \nabla T) + L \frac{\partial w_f}{\partial t} \quad (3-15)$$

Here, ρ , C and λ are density, heat capacity and thermal conductivity of the system, ∇ is the spatial derivative term, and L is latent heat of fusion (333.5 kJ/kg). First term on the right side of equation 3-15 solves the distribution of temperature using the gradient of temperature and heat conduction property of the body. Last term of this equation acts as the sink/source based on the direction of phase transition of water. During freezing, water releases the heat of fusion and this term acts as a source. While during melting water consumes heat of melting and this term acts as a sink. Notice that equation 3-15 uses total mass of water (w_f) that gets frozen or melted during phase transition. Total mass of phase transitioning water (w_f) can be computed from the volume of water that undergoes phase transformation. It is done by utilizing a pore size distribution curve of a porous structure. Pore size distribution (PSD) is the volume distribution curve of the pore of individual sizes and can be measured using Mercury Intrusion Porosimetry (MIP) or other techniques. Considered pore size distribution of a sample concrete is shown in Figure 3-2.

The total volume of the pore is given by equation 3-16 (Zuber & Marchand, 2004),

$$v_p = \int_{\infty}^r \frac{d\phi}{dr} dr \quad (3-16)$$

Note that equation 3-16 integrates the function from ∞ to r . This equation computes the cumulative pore volume from the largest pore to the smallest. It is done in this order since, at the initial stage of MIP, mercury penetrates the largest pores of concrete. Penetration into smaller pores occurs under increased pressure. Therefore, the incremental pore volume ($d\phi$) for a radius increment of (dr) is provided in an order from largest to smallest pores. This order is also valid in case of freezing as well, since the pores of concrete get frozen in a successive order from larger to smaller pores. In other words, largest pores get frozen first while the smallest pores freeze at a lower temperature. The value of $\frac{d\phi}{dr}$ can be estimated from the pore size distribution curve by calculating the slope of ϕ between two successive pore radii, (r). It was also experimentally confirmed and shown in equation 3-7 that there exists a thin layer of water adsorbed on the pore wall. This layer of water does not get frozen and stay supercooled at subzero temperatures (Fagerlund, 1973). The volume of adsorbed water is calculated using equation 3-17.

$$v_a = \int_{\infty}^r \frac{2r_a}{r} \times \frac{d\phi}{dr} dr \quad (3-17)$$

Now the actual mass of water that gets frozen can be calculated by subtracting equation 3-17 from equation 3-16 and multiplying by water density, ρ_w . It gives,

$$\begin{aligned} w_f &= \rho_w(v_p - v_a) = \rho_w \left(\int_{\infty}^r \frac{d\phi}{dr} dr - \int_{\infty}^r \frac{2r_a}{r} \frac{d\phi}{dr} dr \right) \\ &= \rho_w \int_{\infty}^r \left(1 - \frac{2r_a}{r} \right) \frac{d\phi}{dr} dr \end{aligned} \quad (3-18)$$

Finally, the time derivative of the equation should be calculated to use in equation 3-15 and can be found using chain rule of differentiation,

$$\frac{dw_f}{dt} = \frac{dw_f}{dr} \times \frac{dr}{d\theta} \times \frac{d\theta}{dt} = -\rho_w \left(1 - \frac{2r_a}{r}\right) \frac{d\phi}{dr} \times \frac{64}{(\theta + k_b c_m)^2} \times \frac{dT}{dt} \quad (3-19)$$

Substituting $\frac{dw_f}{dt}$ from equation 3-19 in equation 3-18 yields,

$$\rho C \frac{\partial T}{\partial t} = \nabla \cdot (\lambda \nabla T) + \left(-L\rho_w \left(1 - \frac{2r_a}{r}\right) \frac{d\phi}{dr} \times \frac{64}{(\theta + k_b c_m)^2} \times \frac{dT}{dt} \right)$$

$$\vartheta \frac{\partial T}{\partial t} = \nabla \cdot (\lambda \nabla T) \quad (3-20)$$

Where $\vartheta = \left(L\rho_w \left(1 - \frac{2r_a}{r}\right) \times \frac{64}{(\theta + k_b c_m)^2} \frac{d\phi}{dr} + \rho C \right)$. It is convenient to amount of water and ice in concrete as volume fraction of pore. Considering S_i as the ratio of volume of ice and pore and S_w as the ratio of volume of water and pore defined as,

$$S_i = \frac{V_i}{n} = \frac{w_f}{\rho n} \text{ and } S_i + S_w = 1 \quad (3-21)$$

where V_i is the volume of ice in the system and n is total porosity. These expressions can be used to compute volume averaged material properties of the system. Accordingly, the heat capacity (c) and thermal conductivity can be computed using (Zuber & Marchand, 2004),

$$\lambda = n(S_w \lambda_w + S_i \lambda_i) + (b - n) \lambda_s \quad (3-22)$$

and,

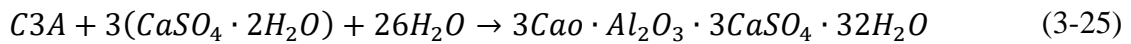
$$C = n(S_w C_w + S_i C_i) + (b - n) C_s \quad (3-23)$$

here, b is Biot's coefficient. Equation 3-20 can solve the heat distribution in a body undergoing phase transition. However, this equation is coupled with the current concentration of sulfate inside the pores by the coupling term $k_b c_m$. The molal

concentration of sulfate can be estimated by solving the mass transfer equation of sulfate. As previously stated, the mass transfer of sulfate ions in concrete is solved using a model previously published by the authors (Islam et al., 2018). A brief description of the model is provided in the following section.

Mass Transport

It is necessary to solve the mass transfer equation in concrete due to the coupling between heat transfer equation and freezing point depression caused by sulfate concentration. SA gets triggered after diffused sulfate gets in contact with tricalcium aluminate (C3A) and forms secondary ettringite. The reaction between SA and sulfate ions occurs in two stages. At first, diffused sulfate reacts with calcium hydroxide ($Ca(OH)_2$) and produces gypsum ($CaSO_4 \cdot 2H_2O$). Then the precipitated gypsum produces ettringite ($3CaO \cdot Al_2O_3 \cdot 3CaSO_4 \cdot 32H_2O$). This series of reactions is shown in equations 3-24 and 3-25.



It is experimentally confirmed that ettringite forms in capillary pores not in the gel pores. Generally, capillary pores contribute up to 50% of the total porosity (Basista & Weglewski, 2009). Mass transport through capillary pores occurs mainly by diffusion mechanism governed by Fick's law. Hence, the amount of sulfate diffused into concrete is given by (Islam et al., 2018),

$$\frac{d[S]}{dt} = \nabla \cdot \left\{ D'_s S_w \nabla \left(\frac{[S]}{S_w} \right) \right\} + D_w \frac{[S]}{S_w} \nabla S_w - k_1 [CA][S] \quad (3-26)$$

here, [S] is molar concentration of sulfate, $D'_s = D'_s(S_w, T)$ is diffusion constant, which is a function of the degree of saturation, S_w , and temperature T , D_w is the diffusion

constant of moisture migration inside the concrete, $[CA]$ is the molar concentration of calcium aluminate and k_1 is the rate of reaction of equation 3-24. The first term on the right side of equation 3-26 estimates the amount of diffused sulfate based on current moisture content, the second term determines the convection of sulfate due to moisture transport and the last term performs as a sink and determines the amount of sulfate consumed due to the reactions given by equations 3-24 and 3-25. In this work, it was assumed that the body is completely saturated to disregard the interaction between air/water and air/ice interaction. Due to this assumption, Sw in the body becomes 1 and the second term vanishes since there is no gradient of moisture inside the body. Hence, equation 3-26 can be rewritten as,

$$\frac{d[S]}{dt} = \nabla \cdot (D'_s \nabla [S]) - k_1 [CA][S] \quad (3-27)$$

Since the diffused sulfate reacts with C3A initially present in the concrete sample and does not get introduced from outside of the body, the temporal variation of the concentration of C3A is an ordinary reaction equation given by,

$$\frac{d[CA]}{dt} = -\frac{k_1}{q} [CA][S] \quad (3-28)$$

where, q is the stoichiometric coefficient of the reaction. Now the rate of formation of ettringite ($[Et]$) is obtained using equation 3-29.

$$\frac{d[Et]}{dt} = -k[S]([CA]_i - [Et]) \quad (3-29)$$

Here it is noteworthy that, the solubility of substances at subzero temperature is negligible. Hence, the sulfate diffusion continues when the temperature is above (0°C). In other words, sulfate diffusion is stopped as soon as the temperature at individual solution node reaches 0°C from above zero temperature. The diffusion process resumed when the boundary temperature passed 0°C from subzero temperature. This method is

applied because it can be safely assumed that all the pore water of the surrounding environment reached subzero temperature and froze. This ultimately will stop further diffusion of sulfate ions from outside.

Equations 3-20, 3-27, 3-28, and 3-29 solves the coupled SA and F-T attack on concrete. Nevertheless, modeling the damage process requires the stress generated due to this coupled degradation process. This will be discussed in the following section.

Modeling Stress and Strain

This section is devoted to modeling the pore stress accumulation in the solid matrix of concrete. Afterward, this stress is utilized in modeling the damage. To this end, the equations for pore crystallization in the section describing the freezing theory are recalled. Stress experienced by a freezing pore averaged over entire volume is expressed as (K. Li, 2016),

$$\langle \sigma_p \rangle = S_i p_i + S_w p_w \quad (3-30)$$

here the angular bracket denotes an average over the entire volume. Relation between p_i and p_w can be found using equation 3-6. However, in absence of traction pressure in water can be assumed to be equivalent to the atmospheric pressure (K. Li, 2016) then equation 3-29 after substituting p_i from equation 3-6 is reduced to,

$$\langle \sigma_p \rangle = \frac{2\gamma S_i}{r} \quad (3-31)$$

Now the stress in solid can be calculated by integrating the pore pressure over the temperature range from reference freezing temperature, T_f to the current temperature ($T < 0^\circ\text{C}$). The average stress in the solid matrix is then obtained by (K. Li, 2016),

$$\sigma_{ft}|_{T_f \rightarrow T} = \frac{n}{1-n} \int_{T_f}^T \left(\frac{2\gamma S_i}{r} \times \frac{dS_i}{dT} \right) dT \quad (3-32)$$

Thermal expansion (ε_T) is found by multiplying thermal expansion coefficient (α) of the system with the change in temperature from the reference temperature ($T - T_{ref}$). Hence, strain due to temperature change is given by (Zuber & Marchand, 2004),

$$\varepsilon_T = \frac{1}{3} \alpha * (T - T_{ref}) \quad (3-33)$$

Finally, the strain due to SA (ε_{SA}) can be calculated using molar volumes of molar volume and current concentrations of ettringite, C3A (Basista & Weglewski, 2009).

$$\varepsilon_{SA} = \frac{1}{3} \left(\frac{[Et] \left(\frac{v_e}{1-n_e} \right) + [CA]v_a}{[CA]_i v_a} - (1 + fn) \right) \quad (3-34)$$

Here, $[Et]$ and $[CA]$ are current concentrations of Ettringite and C3A, $[CA]_i$ is the initial concentration of C3A in the system, v_e and v_a are molar volumes of ettringite and C3A, n and n_e are the porosity of ettringite and concrete, and b is the Biots coefficient. The values of v_e , v_a and n_e are taken as $725.1 \text{ (cm}^3/\text{mol)}$, $88.8 \text{ (cm}^3/\text{mol)}$ and 0.18 respectively (Basista & Weglewski, 2009), f is the fraction of porosity that gets filled due to precipitation of ettringite taken as 0.05 (Idiart, López, & Carol, 2011). After Ettringite gets deposited, the updated porosity becomes,

$$n_{updated} = \max((n_i - \alpha_s([CA]_i - [CA])), 0) \quad (3-35)$$

here, α_s is related to the concentration and molar volume of reacting species. Its value is taken as $113.3 \text{ cm}^3/\text{mol}$. Note that, porosity change equation 3-35 only affects the capillary pores that ranges between $10\mu\text{m} - 50\text{nm}$. Therefore, at each time step, pores having a radius of 50nm and above is updated based on the degree of reaction extent.

Equations 3-32, 3-33, and 3-34 can be used in static equilibrium equation to obtain the overall stress-strain condition of the whole system due to the combined effect of SA, F-T and variation in temperature.

$$\left\{ \frac{1}{2} C_{ijkl} \varepsilon_{kl} - \frac{E}{3(1-2\nu)} (\alpha * (T - T_{ref}) + \varepsilon_{SA}) \delta_{ij} - \sigma_s \delta_{ij} \right\}_{,j} = 0 \quad (3-36)$$

Here, C_{ijkl} is the elasticity tensor, δ_{ij} is Kronecker delta. $\delta_{ij} = 1$ when $i = j$ and $\delta_{ij} = 0$ when $i \neq j$. Stress-Strain distribution in the system can be obtained by solving equation 3-36 and is used in the damage function, explained in the following section, to determine the degree of damage of the system. Finally the porosity change due to material deformation can be evaluated using,

$$\frac{dn}{dt} = (b - n_{updated}) \left(\frac{d\varepsilon_{vol}}{dt} + \frac{1}{K_m} \frac{d\sigma_{ft}}{dt} - \alpha \frac{dT}{dt} \right) \quad (3-37)$$

Here, K_m is the compressibility modulus of the solid matrix and a value of $10.4GPa$ is adopted. Note that this equation is coupled with the change in porosity due to SA by $n_{updated}$ term.

Governing Equations for Coupled TCM Behavior Under SA and FT

Until now we discussed different aspects of the development part of the coupled SA and F-T damage process. The developed model includes the coupling control equations of the interaction of sulfate migration, the reaction between sulfate and C3A, ice formation, skeleton deformation, and heat transfer. Derivation of the constitutive equations has been discussed in the above sections. A summary of the set constitutive equations to capture this coupled phenomena is given below,

$$\vartheta \frac{\partial T}{\partial t} = \nabla \cdot (\lambda \nabla T) \quad (3-38a)$$

$$\frac{d[S]}{dt} = \nabla \cdot (D'_s \nabla [S]) - k[CA][S] \quad (3-38b)$$

$$\left\{ \frac{1}{2} C_{ijkl} \varepsilon_{kl} - \frac{E}{3(1-2\nu)} (\alpha * (T - T_{ref}) + \varepsilon_{SA}) \delta_{ij} - \frac{1}{3} \sigma_s \delta_{ij} \right\}_{,j} = 0 \quad (3-38c)$$

Note that, this equation set is highly coupled with one another. For example, equation 3-38a solves the heat transfer and phase transition in the sample, heat transfer term is embedded in ϑ . Temperature distribution calculated by equation 3-38a is utilized in both equation 3-38b and 3-38c. Equation 3-38b is the diffusion-reaction equation for sulfate migration, and solves the amount of sulfate ingressed into concrete and depletion of $[CA]$ and $[S]$ due to reaction between them. This equation uses the temperature solution from 3-38 a to update the sulfate diffusion coefficient (D'_s) at every time step. This updated sulfate diffusion coefficient is used to calculate the distribution of sulfate. Finally, equation 3-38c depends on both 3-38a and 3-38b and solves the stress and strains generated due to coupled SA, F-T and temperature variation throughout the system.

Model Validation

The preceding coupled equation set, equation 3-38a through 3-38c, is so complicated and intertwined that the analytical solutions can hardly be obtained. Therefore, the equation set is solved numerically with the help of Matlab® Partial Differential Equation (PDE) solver. Matlab PDE solver is a robust interactive environment for modeling and solving coupled nonlinear problems. Matlab PDE solver utilizes a finite-element method (FEM) and is powerful enough to solve complex nonlinear coupled PDEs like equation set 3-38.

The targets in this finite-element analysis are: (1) to validate the proposed constitutive equations by a comparing the simulation results with available experimental

data; (2) to predict the temperature and sulfate distributions, amount of frozen water inside the simulation domain.

A simulation scheme was set up in order to reproduce the experimental results provided by K. Li (K. Li, 2016). The author presented an experimental investigation that studied the F-T damage on concrete. Two concrete samples having w/c ratio of 0.3 and 0.5 were selected for this study. First, the MIP data of concrete with the stated w/c ratios are extracted from (Gong, Zhang, Sicat, & Ueda, 2014) and plotted in Figure 3-2.

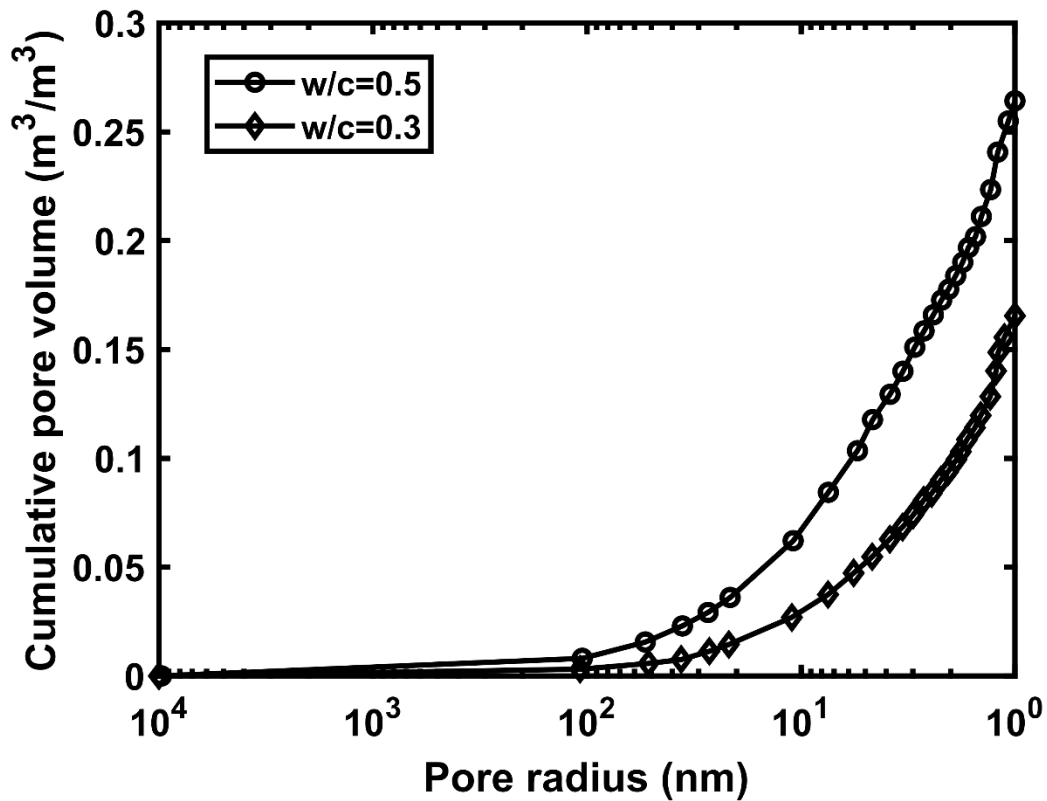


Figure 3-2. Pore size distribution of concrete with w/c ratios of 0.3 and 0.5 (This plot was drawn by extracting PSD data from Gong et al.(Gong et al., 2014))

Figure 3-2 shows PSD of two sample concretes having w/c ratios of 0.3 and 0.5. It can be seen from this figure that the concrete sample having w/c ratio of 0.5 has a final cumulative pore volume of 0.26 whereas this value is 0.16 for the concrete sample with

w/c ratio of 0.3. Therefore, it shows the effect of w/c ratio on the overall porosity of the concrete. However, this is a well-established fact for concrete. The PSD curve also shows that the pores having a radius of 100nm and above forms about 7-8% of the total porosity for both concrete samples and the rest of the porosity comes from the pores having a radius less than 100nm. Henceforth, the mortar sample with w/c ratio of 0.3 will be called as Sample 1 and the sample with w/c ratio of 0.3 will be named as sample 2.

The pore size distribution data was utilized in the validation model. One-quarter of a mortar cube with dimensions $25\text{mm} \times 25\text{mm} \times 25\text{mm}$ is used as a simulation domain to reduce the computation time. The simulation domain is shown in Figure 3-3.

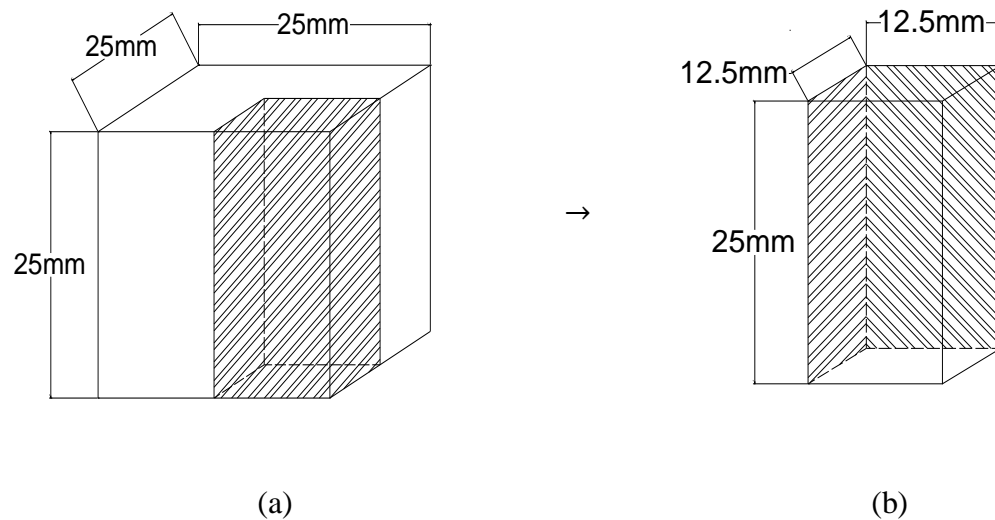


Figure 3-3. a) Full-size mortar sample, b) Simulation domain for validating the proposed model

The boundaries of the simulation domain as shown in Figure 3-3b is identified as top-bottom, left-right, and front-back boundaries. Accordingly, the back and left boundaries are considered as symmetric due to being connected to the other parts of the full-size sample shown in Figure 3-3a. The symmetric boundaries are marked by the shaded area and are not directly accessible to the environmental factors such as temperature and

SA. Therefore, all the boundary conditions are applied on top, bottom, front and right boundaries of the domain. The origin of the Cartesian coordinate system is placed at the front right corner of the simulation domain. For the mechanical equilibrium equation, normal displacements for the symmetric boundaries are set to zero. Applied boundary and initial conditions are listed in Table 3-1.

Table 3-1. Initial and boundary conditions

Boundary condition		Initial condition	
Boundaries Top, Bottom, front and right		[CA]	$82.5 \text{ mol} \cdot \text{m}^{-3}$
[S]	$350 \text{ mol} \cdot \text{m}^{-3}$	[S]	0
T_b	$10 - \frac{t}{560} \text{ [}^\circ\text{C]}$, (t in seconds)	T	283.15 K (10°C)
Boundaries: Left and back		σ and ε	0
Normal displacement	0		

Little (Little & Nair, 2009) summarized in a report that sulfate concentration in the soil could reach up to 10,000ppm or mg/kg of the soil mass. Moreover, typical soil moisture content ranges from 10 to 35% by mass. Therefore, in a soil mass weighing 1 kg there will be 100 to 350g of water in natural condition. Consequently, 10,000mg or 10g of sodium sulfate will be dissolved in say 200g of water (taking the mid-range moisture content). Since, the density of water is $1\text{g}/\text{cm}^3$ so, 10g of sodium sulfate will be dissolved in say 200cm^3 of water. The molar weight of sodium sulfate is $142.04\text{g}/\text{mol}$. As a result, 10g of sodium sulfate is equivalent to 0.071mol. It means that 0.071mol of sodium sulfate is dissolved into 200cm^3 or 0.0002m^3 . This results in the molarity of the sodium sulfate in

the soil as $0.071/0.002 = 355 \text{ mol/m}^3$. Therefore, a sulfate boundary condition of 350 mol/m^3 is adopted.

Different material properties adopted for simulating the coupled equation set 3-40 is provided in Table 3-2.

Table 3-2. Material properties

Thermal properties	Mortar	Water	Ice
Density [g/cm^3]	2.14	1	0.916
Thermal expansion coefficient, $\alpha[k^{-1}]$	30×10^{-6}	$(-9.2 + 2.07 \times T) \times 10^{-5}$	12.28×10^{-5}
Thermal conductivity, $\lambda [W/m/K]$	0.93	0.55	2.2
Heat capacity, $C[J/g/K]$	0.84	4.22	2.11
Surface tension of water $\gamma[N/m]$	N/A	0.04	N/A
Latent heat of water, $L[J/g]$	N/A	333.5	N/A
Biot Modulus	0.461		
Total porosity, n	0.18 (for w/c = 0.3) 0.28 (for w/c = 0.5)		
Fracture energy, $G_f[N/mm]$	0.05		
Elastic modulus, $E[GPa]$	20.2 (for w/c = 0.3) 10.1 (for w/c = 0.5)		

After simulating the constitutive equation set 3-38 for two different mortar samples sample1 and sample2, the ice content (S_i) as a percent fraction of pore volume are validated against experimental data published by Li (K. Li, 2016). The simulation and experimental results are plotted and displayed in Figure 3-4.

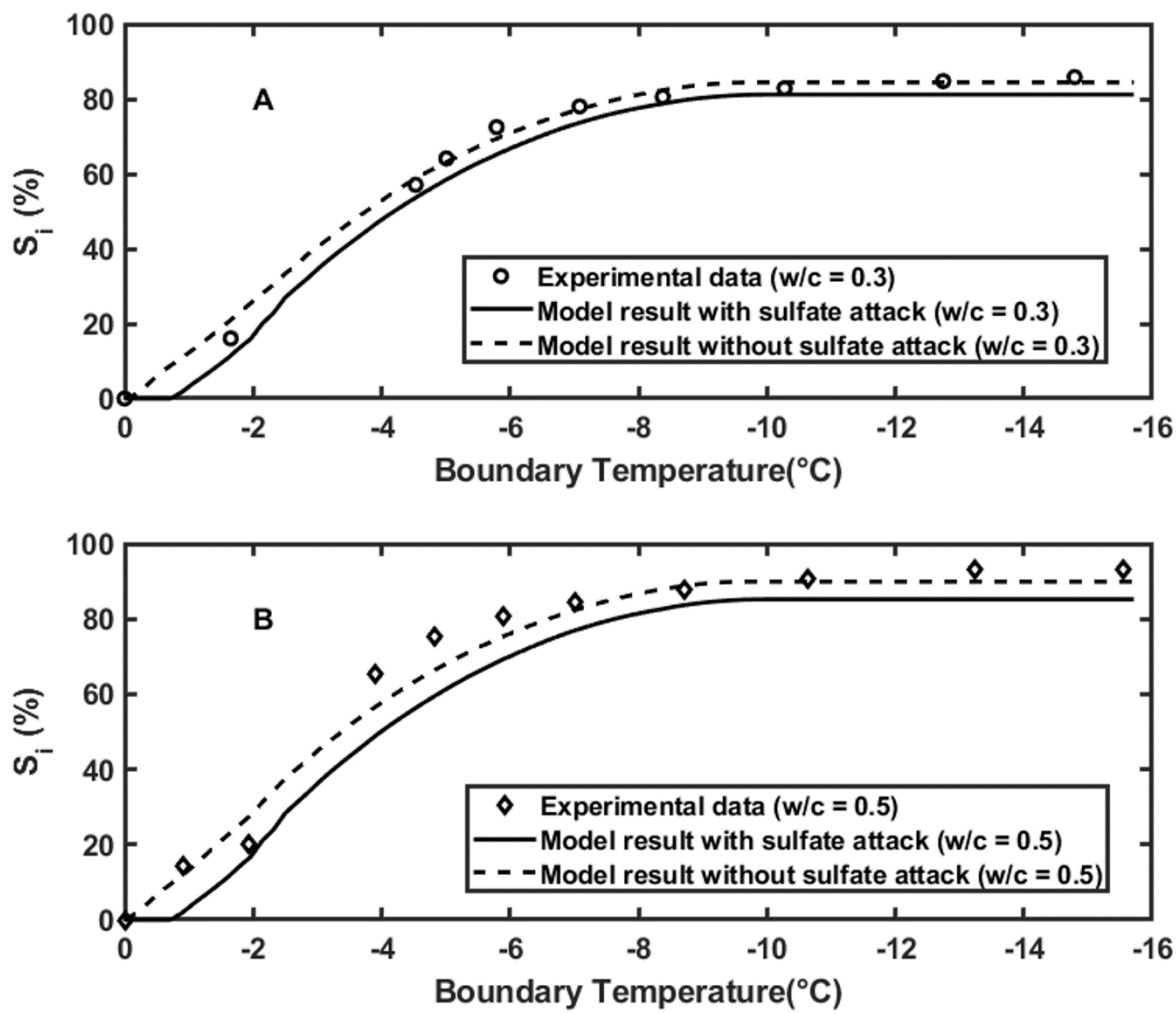


Figure 3-4. Ice fraction in mortar sample with, a) Sample1 and b) Sample2

Figure 3-4 shows the variation of ice content with and without sulfate reaction in a mortar sample as a function of boundary temperature. Note that prior to applying the effect of F-T, 180 days of SA is simulated to observe the effect of SA on F-T. This figure shows that the variation of frozen water contents of the two mortars has a similar trend. In both samples the fraction of ice content increases with the decrease in boundary temperature. It happens because water content dwelling inside larger pores gets transformed first. Further reduction in temperature causes phase transformation of water inside the smaller pores. This is because of the effect of freezing point depression due to pore size reduction.

However, the slope increases until the boundary temperature reaches -4°C . After crossing this temperature threshold, the slope starts decreasing. This nonlinearity in the porous ice content is due to the fact that water in larger pores having radii of 100nm or more releases their heat of fusion due to phase transition until the boundary temperature reaches -4°C . This released heat from phase transformation keeps the surrounding water from freezing, which requires further reduction in temperature. Once the larger pores get frozen, the amount of heat generated due to phase transition is reduced. This is because smaller pores contain relatively less amount of water compared to the larger pores. Further investigation of this figure shows that, there is no variation in ice content after the boundary temperature exceeds -9°C , meaning that no more water got transformed into ice after this temperature. Hence, it can be stated that -9°C is the minimum temperature limit for transforming all the pore water of concrete into ice. From this point forward, this situation is defined as the ice saturation point, when no more free water is available for phase transformation. At the ice saturation point concrete experiences the maximum stress due to freezing. The predicted results from the model qualitatively agree very well with the test results shown by Li (K. Li, 2016). Afterward, a regression analysis is conducted to determine the correlation between the model outputs and experimental results. Excellent correlation of 99% is obtained for both mortar samples when simulated without the effect of sulfate attack. However, the simulation results with sulfate attack yielded a correlation value of 86%. This is expected since the experimental results were obtained using a mortar sample saturated with pure water and no sulfate content was included. This figure also shows the effect of sulfate solution on freezing point depression. For both samples 1 and 2, freezing of pore water started when boundary temperature reached -0.9°C . Final porous ice fraction from

the experiment and simulation results with and without sulfate attack is shown in Table 3-3.

Table 3-3. Pore ice content at the experiment and simulation

Data source	Sample 1	Sample 2
Experiment	85.8%	93.3%
Without sulfate attack	84.4%	95%
With sulfate attack	81%	85%

Due to the appearance of SA on sample1 and sample2, about 5% and 8% less ice is produced because of the freezing point depression effect, respectively. This reduction in ice content comes from the reduction of porosity due to the deposition of expansive ettringite as a result of SA.

Results and Discussion

Variation in Temperature at The Center of the Specimen

In the preceding section it was shown that the model agrees well with the experimental results. Now it is attempted to evaluate the effect of SA on phase change inside pores. Therefore, the temperature variations at the center [12.5mm, 12.5mm, 12.5mm] of the specimen for the cases with and without sulfate attack is shown in Figure 3-5.

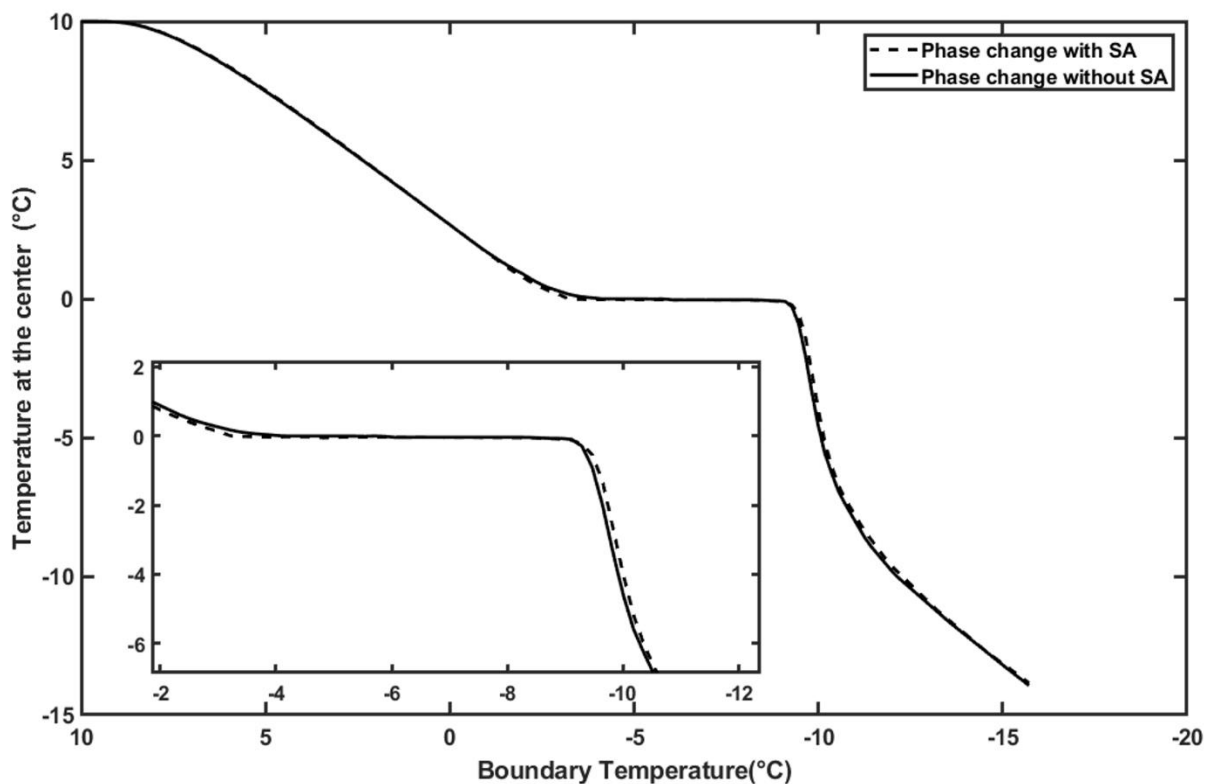


Figure 3-5. Freezing with and without sulfate attack.

A zoom-in view of the plot is also provided in the figure to facilitate the observation of the effect of SA on phase transition. It can be seen that while the boundary temperature is -3.2°C the local temperatures at the center are 0°C when SA is active on the domain and 0.16°C when only F-T is acting on the domain (pure water). Therefore, it is evident that the temperature at the center is relatively lower at the beginning of freezing when SA is acting on the specimen compared to the case without SA. This is due to the fact that the freezing temperature of the sulfate solution is lower than that of pure water. Consequently, sulfate containing pore water starts freezing at a lower temperature compared to pure water. This depression of freezing point is calculated using the coupling term $k_b c_m$. Analysis of the falling leg of temperature curve at the center reveals that, when the boundary temperature reaches -10°C the temperatures at the center for the cases with pure water and

sulfate solution are -4.5°C and -4°C , respectively. This means that temperature curve of sulfate containing pore water follows the temperature curve of pure water. Since the temperature is reduced at a rate of $\frac{1}{560}^{\circ}\text{C/s}$, the temperature curve of falling leg of porous sulfate solution lags pure water by $0.5 \times \frac{1}{560} = 280\text{s}$. This is also because of the freezing point depression due to sulfate solution, that cause the sulfate solution to freeze at a lower temperature compared to pure water.

Hysteresis of Solidification and Melting Due to Freeze-Thaw

Hysteresis is a property of a material that is defined by the reliance of the state of a system on its history. In this case the dependence of phase change in the porous water on its current phase is of interest. In order to observe the hysteresis of freezing and melting of water the boundary temperature is first reduced from 10°C to -15.7°C in 4 hours. After that, the boundary temperature is raised from -15.7°C to 10°C in 4 hours. After simulating the domain with above mentioned boundary condition the ice content in porous structure is evaluated for sample 1 ($w/c = 0.3$) in freezing and thawing stages and is shown in Figure 3-6. Note that frost generation after sulfate attack is considered for this simulation.

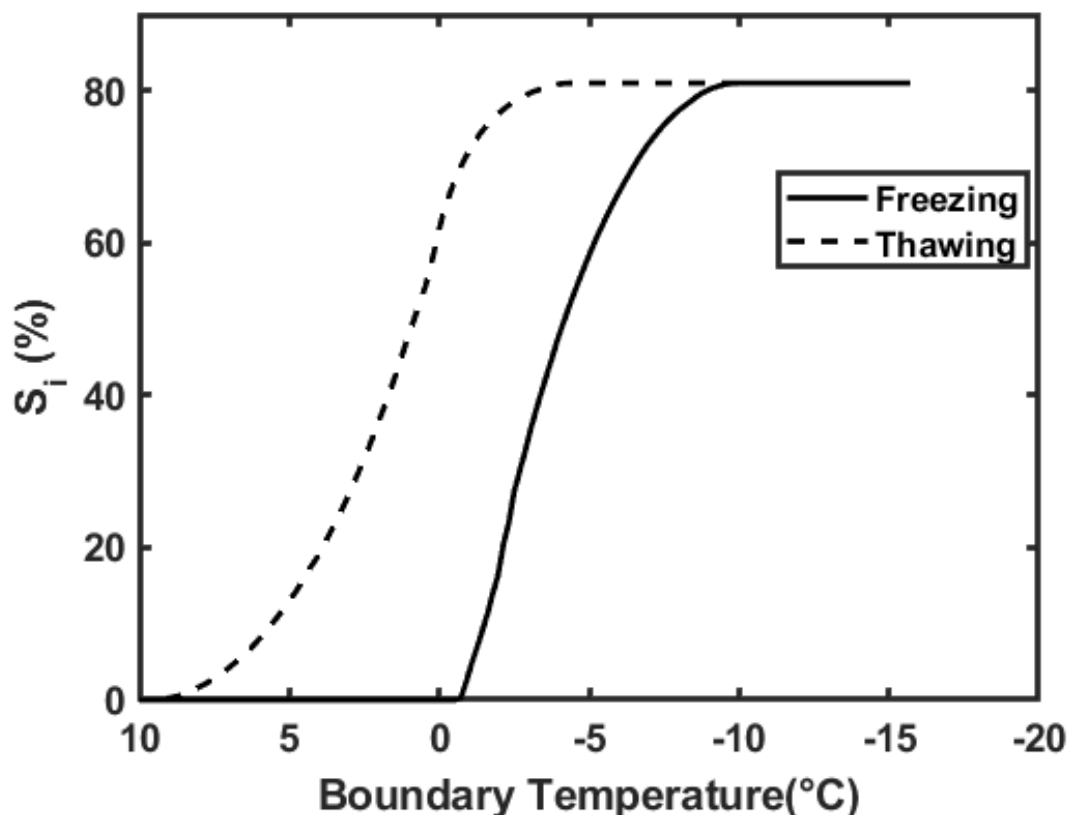


Figure 3-6. Hysteresis of solidification and melting due to fluctuation in temperature in pores

Due to the latent heat of porous water, the same temperature does not yield the same percentage of frost inside the pores. From Figure 3-6, it can be seen that when the temperature is being reduced from 10°C frost generation starts at -0.9°C . In contrast, melting gets initiated at around -3.2°C when the temperature is being increased from -15.7°C . Complete melting occurs around 8.2°C . This means that if the ambient temperature does not rise above 8.2°C , there will be residual ice, and concrete pores will be under stress due to this residual frost. As previously discussed, complete freezing occurs around -9°C , causing maximum frost generated stress. Therefore, the concrete structures in freezing regions experience frost generated stress in the temperature range of -9°C to 8.2°C . In other words, concrete experiences frost-produced expansive stress in the

temperature range of -9°C to 8.2°C . This large temperature range is all caused by the hysteresis of F-T of porous water. Of course, surrounding temperature may get further reduced, but, once all the free water gets frozen no further stress gets added to the existing stress due to frost.

Variation of Sulfate Concentration Due to F-T Damage

Two different situations, one with one cycle of F-T and one without F-T, were simulated in order to observe the effect of damage due to F-T on sulfate diffusion. The results are plotted in Figure 3-7. In this case as well, the sulfate content in concrete is evaluated for sample 1 ($w/c = 0.3$).

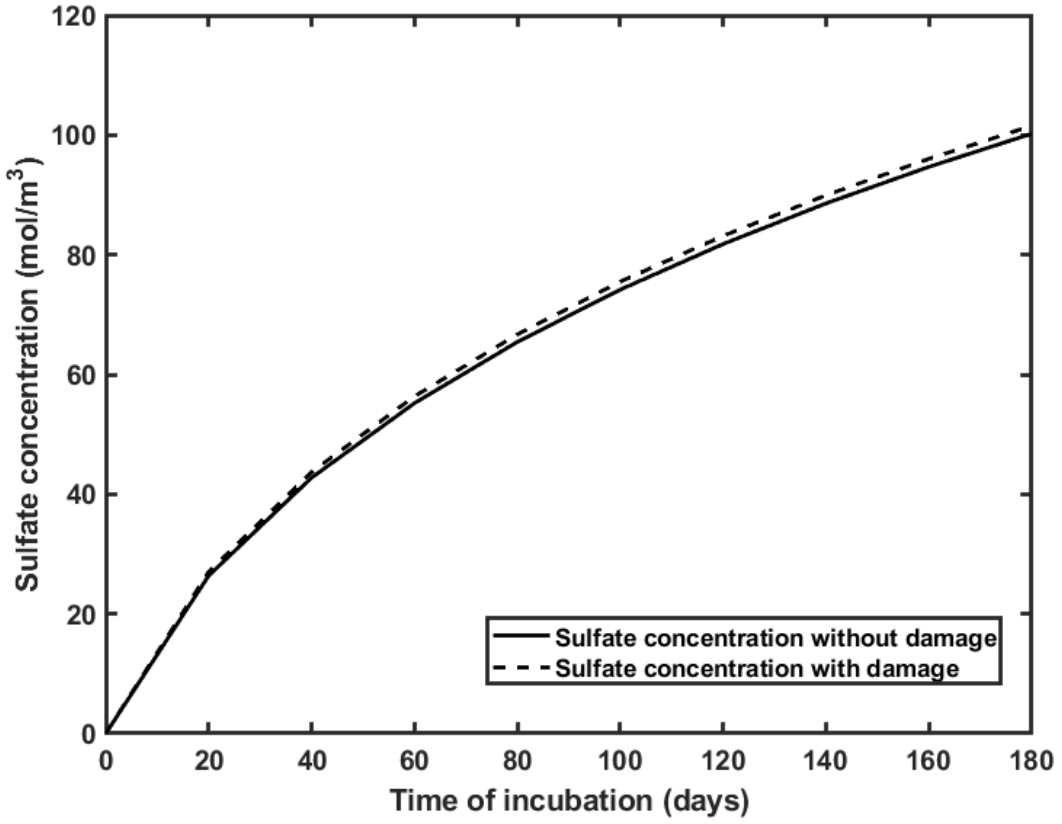


Figure 3-7. Effect of F-T damage on sulfate concentration inside concrete

From Figure 3-7, it can be seen that the damage due to F-T has an appreciable effect on sulfate diffusion inside concrete. This figure shows that at the end of 180 days of incubation, the amounts of sulfate diffused inside concrete with and without F-T damage are 101.5432 mol/m^3 and 100.23 mol/m^3 , respectively. This relatively higher (1.3%) amount of sulfate gets accumulated in concrete due to increase in diffusivity as a result of damage after one cycle of F-T.

Conclusion

A poromechanics based mathematical model is developed to predict the interaction of F-T and SA. Phase transitions within the pore space along with the chemical reactions of SA are considered at the pore scale. The system of non-linear equations is solved numerically using FEM. The coupled interaction of SA and F-T is considered using the change in porosity due to the combined effect of these environmental attacks. The present model is a first step in the development of a comprehensive framework for the numerical prediction of the damage in concrete due to coupled SA and F-T.

Validation of the proposed TCM framework is conducted by simulating an experiment of two mortar samples having different porosities, involving mortar specimens subjected to F-T and SA. It was shown that, simulation results matched very well with the experimental results when mortar pores were saturated with pure water. For pure water, the correlation between experimental and simulation results was found to be 99%, which is excellent.

It was observed from the model results that concrete pores get saturated by ice at a temperature of -9°C and due to the hysteresis effect of solidification and melting of

porous water, complete melting of pore water occurs around 8.2°C. Between these temperatures, there will be residual ice in the concrete pores and continue exerting tensile stress on the pore walls until the volume of ice and melted water reduces below the volume of pores.

Analyzing the interior temperature against boundary temperature shows that the sulfate solution reduced the freezing point temperature. The temperature profile of the sample experiencing SA lagged by 280s. Note that this is an accelerated F-T simulation and the boundary temperature reduced at a rate of $\frac{1}{560}$ °C. In other words, the variation of 1°C occurred in 9.33 minutes. This is pretty fast compared to environmental temperature variations. Therefore, frost generation in environmental conditions will be much more alleviated by the SA. Finally, the analysis of sulfate concentration inside concrete reveals that 1.3% more sulfate gets accumulated inside concrete due to damage caused by one cycle of F-T.

REFERENCES

- Al-Dulaijan, S. U., Maslehuddin, M., Al-Zahrani, M. M., Sharif, A. M., Shameem, M., & Ibrahim, M. (2003). Sulfate resistance of plain and blended cements exposed to varying concentrations of sodium sulfate. *Cement and Concrete Composites*, 25(4–5), 429–437. [https://doi.org/10.1016/S0958-9465\(02\)00083-5](https://doi.org/10.1016/S0958-9465(02)00083-5)
- Basista, M., & Weglewski, W. (2009). Chemically assisted damage of concrete: A model of expansion under external sulfate attack. *International Journal of Damage Mechanics*, 18(2), 155–175. <https://doi.org/10.1177/1056789508097540>
- Bazant, Z. P., Chern, J. C., Rosenberg, A. M., & Gaidis, J. M. (1988). Mathematical Model for Freeze-Thaw Durability of Concrete. *Journal of American Ceramic Society*, 9(71), 776–783.
- Cefis, N., & Comi, C. (2017). Chemo-mechanical modeling of the external sulfate attack in concrete. *Cement and Concrete Research*, 93, 57–70. <https://doi.org/10.1016/j.cemconres.2016.12.003>
- Duan, A., Chen, J., & Jin, W. (2013). Numerical Simulation of the Freezing Process of Concrete. *Journal of Materials in Civil Engineering*, 25(9), 1317–1325. [https://doi.org/10.1061/\(ASCE\)MT.1943-5533.0000655](https://doi.org/10.1061/(ASCE)MT.1943-5533.0000655)
- Ebbing, D. D., & Gammon, S. D. (2009). *General Chemistry*.
- Fagerlund, G. (1973). Determination of pore size distribution from freezing-point depression. *Matériaux et Constructions*, 6(3), 215–225. <https://doi.org/10.1007/BF02479036>
- Gong, F., Zhang, D., Sicat, E., & Ueda, T. (2014). Empirical Estimation of Pore Size Distribution in Cement, Mortar, and Concrete. *Journal of Materials in Civil*

- Engineering*, 26(7), 04014023. [https://doi.org/10.1061/\(ASCE\)MT.1943-5533.0000945](https://doi.org/10.1061/(ASCE)MT.1943-5533.0000945)
- Idiart, A. E., López, C. M., & Carol, I. (2011). Chemo-mechanical analysis of concrete cracking and degradation due to external sulfate attack: A mesoscale model. *Cement and Concrete Composites*, 33(3), 411–423. <https://doi.org/10.1016/j.cemconcomp.2010.12.001>
- Islam, M. A., Golrokh, A., & Lu, Y. (2018). Chemo-mechanical Modeling of Sulfate Attack-induced Damage Process in Cement Stabilized Pavements. *Journal of Engineering Mechanics*.
- Jacobsen, S. and Sellevold., E. J. (1996). Self-healing of high strength concrete after deterioration by freeze-thaw, 26(I), 55–62. [https://doi.org/10.1016/0008-8846\(95\)00179-4](https://doi.org/10.1016/0008-8846(95)00179-4)
- Jallut, C., Lenoir, J., Bardot, C., & Eyraud, C. (1992). Thermoporometry. Modeling and simulation of a mesoporous solid. *Journal of Membrane Science*, 68(3), 271–282. [https://doi.org/10.1016/0376-7388\(92\)85028-H](https://doi.org/10.1016/0376-7388(92)85028-H)
- Jiang, L., Niu, D., Yuan, L., & Fei, Q. (2015). Durability of concrete under sulfate attack exposed to freeze-thaw cycles. *Cold Regions Science and Technology*, 112, 112–117. <https://doi.org/10.1016/j.coldregions.2014.12.006>
- Li, K. (2016). Durability Design of Concrete Structures - Part 1: Analysis Fundamentals.
- Li, Y., Wang, R., Li, S., Zhao, Y., & Qin, Y. (2018). Resistance of recycled aggregate concrete containing low- and high-volume fly ash against the combined action of freeze-thaw cycles and sulfate attack. *Construction and Building Materials*, 166, 23–34. <https://doi.org/10.1016/j.conbuildmat.2018.01.084>
- Little, D. N., & Nair, S. (2009). Recommended practice for stabilization of sulfate-rich subgrade soils. College Station, Texas.
- Long, G., Xie, Y., & Tang, X. (2007). Evaluating deterioration of concrete by sulfate attack. *Journal of Wuhan University of Technology-Mater. Sci. Ed.*, 22(3), 572–576. <https://doi.org/10.1007/s11595-006-3572-6>

- Lu, Y., Garboczi, E., Bentz, D. P., & Davis, J. (2012). Modeling chloride transport in cracked concrete: a 3-D image-based microstructure simulation. *COMSOL Conference 2012, Boston, MA, USA*, 1–15. <https://doi.org/912153>
- Miao, C., Mu, R., Tian, Q., & Sun, W. (2002). 2002 Effect of sulfate solution on the frost resistance of concrete with and without steel fiber reinforcement.pdf, 32, 31–34.
- Neville, A.M. (1981). *Properties of concrete*,. Trans-Atlantic Publications, Inc.
- Niu, D., Jiang, L., & Fei, Q. (2013). Deterioration mechanism of sulfate attack on concrete under freeze-thaw cycles. *Journal Wuhan University of Technology, Materials Science Edition*, 28(6), 1172–1176. <https://doi.org/10.1007/s11595-013-0839-6>
- Papadakis, V. G., Vayenas, C. G., & Fardis, M. N. (1991). Fundamental Modeling and Experimental Investigation of Concrete Carbonation. *ACI Materials Journal*, 88(4). <https://doi.org/10.14359/1863>
- Piasta, W., Marczewska, J., & Jaworska, M. (2015). Durability of air entrained cement mortars under combined sulfate and freeze-thaw attack. *Procedia Engineering*, 108, 55–62. <https://doi.org/10.1016/j.proeng.2015.06.119>
- Puri, B. R., Sharma, L. R., & Lakhdnpal, M. L. (1954). Freezing point of water held in porous bodies at different vapor pressures, 387(1032).
- Scherer, G. W. (1992). Freezing gels. *Journal of Non-Crystalline Solids*, 155, 1–25. [https://doi.org/10.1016/0022-3093\(93\)90467-c](https://doi.org/10.1016/0022-3093(93)90467-c)
- Scherer, G. W. (1999). Crystallization in pores. *Cement and Concrete Research*, 29(December 1998), 1347–1358. <https://doi.org/10.1016/j.jcard.2018.01.096>
- Setzer, M. J. (2000). Micro Ice Lens Formation, Artificial Saturation and Damage during Freeze Thaw Attack. *Materials for Buildings and Structures*, 220. <https://doi.org/10.1002/3527606211>
- Skalny, J. P., Marchand, J., & Odler, I. (2003). *Sulfate Attack on Concrete*. Retrieved from <https://books.google.com/books?id=0ZN-z35qV1sC&pgis=1>

- Sun, W., Zhang, Y. M., Yan, H. D., & Mu, R. (1999). Damage and damage resistance of high strength concrete under the action of load and freeze-thaw cycles. *Cement and Concrete Research*, 29(9), 1519–1523. [https://doi.org/10.1016/S0008-8846\(99\)00097-6](https://doi.org/10.1016/S0008-8846(99)00097-6)
- Wang, D., Zhou, X., Meng, Y., & Chen, Z. (2017). Durability of concrete containing fly ash and silica fume against combined freezing-thawing and sulfate attack. *Construction and Building Materials*, 147, 398–406. <https://doi.org/10.1016/J.CONBUILDMAT.2017.04.172>
- Yang, H., Shen, X., Rao, M., Li, X., & Wang, X. (2015). Influence of Alternation of Sulfate Attack and Freeze-Thaw on Microstructure of Concrete. *Advances in Materials Science and Engineering*, 2015. <https://doi.org/10.1155/2015/859069>
- Zuber, B., & Marchand, J. (2004). Predicting the volume instability of hydrated cement systems upon freezing using poromechanics and local phase equilibria. *Concrete Science and Engineering*, 37, 257–270. <https://doi.org/10.1617/14165>

CHAPTER FOUR: CONCLUSION

Concrete damage due to coupled SA and F-T is prevalent in cold regions having ample amount of free sulfate species in the environment. SA alone is extremely deleterious to concrete structures. SA induced damage in concrete is caused by the reaction between tricalcium aluminate and sulfate ions. Due to this reaction expansive ettringite gets produced and starts damaging concrete as the volume of deposited ettringite exceeds the pore volume. In contrast, F-T damage is caused by expansive stress that is being exerted on the pore walls, since the frozen water has about 9% more volume than water. When F-T damage starts interacting with SA then the damage process becomes highly exacerbated. This thesis presents coupled models for capturing this coupled damage process. First of all, an improved SA model is presented in Chapter two, later this SA model is utilized in coupled F-T and SA damage model. Summary conclusion of the presented models is discussed in this chapter.

Although the process of SA in cementitious materials is well known, a comprehensive mathematical model to predict long-term damage effects is unavailable. Hence, an extensive model is developed to simulate sulfate propagation and predict mechanical stress and damage due to SA. The proposed chemo-mechanical model for cement stabilized subgrade of SA is established with considerations of heat and degree of saturation. The contribution of this paper is that the internal expansion-induced damage effects are calculated by including the unsaturated condition effects and coupled with non-

isothermal heat transfer. It is an improvement from existing SA based damage models, that only considers diffusion in a fully saturated media or an isothermal environment.

Verification of the proposed model is done by simulating an experiment conducted by Condor (Condor et al., 2011). The results from the simulation agreed very well with the experimental results. Further validation of the model is done by comparing stoichiometric coefficients of the reaction. The molar ratio found from simulation is 1.25, whereas the actual value is 1.5. This shows a good match between the reaction and simulation output. In the field, an equilibrium state of moisture distribution can be achieved after few months from the beginning of moisture transport. On the other hand, temperature takes only several days to reach equilibrium. Thus, the layered pavement system achieves equilibrium temperature quite fast compared to moisture migration.

Estimation of the eigenstrain and corresponding mechanical damage along with the stress of cementitious materials under SA is conducted by combining two different models. Concentration threshold for damaged concrete is determined to be 600 mol/m^3 . DP yield criterion is exploited in this model to determine the mechanically damaged zone of cementitious material under SA. Depth of penetration of sulfate diffusion after four months of incubation is calculated to be about 5 mm .

This improved sulfate diffusion model in conjunction with freezing theory of water is employed in the model to predict the coupled damage due to SA and F-T. Phase transitions within the pore space along with the chemical reactions of SA are considered at the pore scale. Interaction of SA and F-T is considered using the change in porosity due to combined effect of these environmental attacks. The present model is a first step

in the development of a comprehensive framework for the numerical prediction of the damage in concrete due to coupled SA and F-T.

Validation of the proposed TCM framework is conducted by simulating an experiment of two mortar samples having different porosities, involving mortar specimens subjected to F-T and SA. It was shown that, simulation results coincide very well with the experimental results when mortar pores were saturated with pure water. For pure water, the correlation between experimental and simulation results was found to be 99%, which is excellent. However, due to the effect of freezing point depression and reduction in porosity caused by sulfate solution the correlation value got lowered by 13%.

It was observed from the model results that concrete pores get saturated by ice at a temperature of -9°C and due to hysteresis effect of F-T of porous water, complete melting of pore water occurs around 8.2°C . Between these temperatures, there will be residual ice in the concrete pores and continue exerting tensile stress on the pore walls until the volume of ice is not less than the volume of pores.

Analyzing the interior temperature against boundary temperature shows that, sulfate solution reduced the freezing point temperature. The temperature profile of the sample experiencing SA lagged by 280s. Note that, this is an accelerated F-T simulation and the boundary temperature reduced at a rate of $\frac{1}{560}^{\circ}\text{C}$ in other words the variation of 1°C occurred in 9.33 minutes. This is pretty fast compared to environmental temperature variations. Therefore, frost generation in environmental conditions will be much more alleviated by the SA. Finally, the analysis of sulfate concentration inside concrete reveals that, 1.3% more sulfate gets accumulated inside concrete due to damage caused by one cycle of F-T.

The developed model can be improved by including the degree of damage based on saturation level. Additionally, inclusion of the effect of concrete microstructure on the freezing process will assist researchers in finding the effects of different phases of concrete such as interfacial transition zone (ITZ). Future iterations of this model will include these phenomenons to offer an improved solution towards designing sustainable concrete structures.